photolithography useful in synthesizing arrays of polypeptides. The Examiner further states that although the specification teaches other means for protecting and deprotecting, the specification does not teach that these methods are used in the instant claimed methods. In particular, the Examiner states that the specification does not teach the use of kinds of radiation other than light and the specific conditions required to use those kinds of radiation in the synthesis of a polypeptide array.

Applicants respectfully traverse this rejection. Applicants strongly disagree with the Examiner's statement that although the specification teaches several methods for protecting and deprotecting functional groups, it does not teach that the protection and deprotection methods are used in the instant claimed method. The specification clearly discloses that protection and deprotection represent steps in the synthesis of a polypeptide array. Teachings related to protection and deprotection methods can be found, for example, at page 10, lines 6-9 (light and electric current), page 17, line 38 to page 18, line 2 (electro-optical and optical methods), page 29, lines 28-35 (x-ray and electron beam lithography), and page 21, lines 7-28 (chemical agents). It has been well established in case law that working examples are not required in order to satisfy the enablement requirement.

> The specification need not contain an example if the invention is otherwise disclosed in such manner that one skilled in the art will be able to practice it without an undue amount of experimentation. *In re Borkowski*, 422 F.2d 904, 908, 164 USPQ 642, 645 (CCPA 1970).

One skilled in the art would readily be able to use a known protection or deprotection technique in the claimed invention based on the teachings of the instant specification.

The following sections discuss in detail why the subject application allows one skilled in the art to practice the instant claims. As is shown below, the present application discloses numerous methods of preparing polypeptide arrays using different substrate protection and deprotection methods. Furthermore, all of these protection and deprotection methods can be used selectively. There is no requirement that Applicants must provide specific working examples of the protection and deprotection methods, because one skilled in the art would be able to practice the invention based on the instant disclosure and on the knowledge of a skilled artisan as of the effective filing date of the application. Taken as a whole, there are a sufficient

number of methods of preparing polypeptide arrays disclosed herein to support a genus claim covering all of these methods.

The Use of Numerous Lithographic Methods Are Enabled

In support of this assertion, Applicants refer to Chapter 4 of "VLSI Technology", Second Edition by S. M. Sze, a copy of which is enclosed as "Exhibit D." VLSI Technology has a copyright date of 1988, which predates the earliest priority claim of this application. Thus, this material was publically available prior to the earliest effective filing date of this application.

VLSI Technology contains a discussion of several lithographic techniques, including electron lithography (also known as electron beam lithography), x-ray lithography and ion lithography. Electron lithography is disclosed to work by bond breaking or formation in a material referred to as a "resist." The electron beam causes bond breaking within a positive resist. A table of materials used as positive resists is shown in Table 2 (page 158 of VLSI Technology). The instant specification teaches at page 29, lines 28 to 35 that sulfonyl moieties are appropriate for use as protecting groups to be removed by an electron beam. VLSI Technology also teaches that masking techniques were already known for use in electron beam lithography (pages 157-160). Similarly, aspects of x-ray lithography are discussed at pages 170-177 of VLSI Technology. Notably, materials used as resists in electron beam lithography are also appropriate for x-ray lithography (page 170). Masks for x-ray lithography are also known. Ion lithography is discussed at pages 177 and 178 of VLSI Technology.

Each of these lithographic methods represents a well-known technique that can be used to deprotect a functional group at a positionally defined location on a solid substrate, after which an amino acid is reacted with the deprotected functional group to build a nascent polypeptide chain. This process of deprotecting a functional group and reacting the deprotected functional group can be repeated numerous times and at various locations on a substrate. Given that lithographic techniques, enabling one to deprotect functional groups at a positionally defined location, were well known as of the earliest effective filing date of the application, and that the present application teaches how a polypeptide array is synthesized (i.e., repeating localized deprotection steps and amino acid addition steps), the instant specification contains adequate teachings in

view of the knowledge of the skilled artisan to enable one skilled in the art to use one of the disclosed lithographic methods to prepare a polypeptide array.

Selective Contact Between A Solution and A Substrate

With respect to methods requiring contact between a substrate and a fluid, Applicants refer to U.S. Patent No. 5,547,839 ("the '839 Patent"), which was previously submitted as "Exhibit B." The Examiner has stated that Exhibit B is not persuasive based on its effective filing date and chain of priority. However, the Examiner has no grounds for not fully considering the subject matter of the '839 Patent, because it is incorporated by reference at page 1, line 31 of the specification. The '839 Patent is based on U.S. Application No. 07/626,730, filed December 6, 1990. The instant application is related by a series of continuation and divisional applications to U.S. Application No. 07/624,114, also filed December 6, 1990. U.S. Application Nos. 07/624,114 and 07/626,730 are both continuations-in-part of U.S. Application No. 07/492,462. Thus, the subject matter disclosed in the '839 Patent was known to Applicants as of the effective filing date of the instant application.

The Examiner's characterization of Figure 11 of the '839 Patent is inaccurate. The Examiner states that Figure 11 illustrates a functionalist apparatus for performing the scanning steps and sequencing reaction steps. The Examiner is directed to column 28, lines 27-38 of the '839 Patent, where the object depicted in Figure 11 is disclosed to be a reaction chamber, with the necessary tubing and valves to control the entry and exit of reagents. One skilled in the art would readily recognize that the size of the reaction chamber can be varied to control how large an area on the substrate is exposed to reagents at a particular time. Also, one skilled in the art would recognize that reaction chambers of varying sizes could be utilized at different stages of polypeptide array synthesis (to expose all or part of a substrate to one or more reagents). Additional methods of controlling which locations are exposed to reagents are disclosed at page 26, lines 18-26 of the instant specification, which include physically dividing or etching a substrate to provide surface features such as trenches, v-grooves and mesa structures.

Given that several methods of controlling the location(s) at which one or more reagents contacted a substrate, one skilled in the art could select from various methods to deprotect a positionally defined location on the substrate and build a polypeptide at that location. Examples

of suitable methods using fluid contact for deprotection include conventional chemical and electrochemical methods. In conventional chemical deprotection, a chemical reagent supplies the necessary energy to deprotect a functional group (see the first full paragraph on page 15 of the Amendment filed June 18, 2002 for a more complete discussion of such chemical reagents). In electrochemical deprotection, the substrate can, for example, be contacted with an electrolyte solution, through which an electric current can subsequently pass.

Summary

Applicants have shown that numerous methods useful in deprotecting a positionally defined region of a substrate are either explicitly taught in the specification, incorporated by reference using an application that was pending as of the earliest effective filing date of the subject application, or known to one skilled in the art on or prior to the effective filing date of the instant application. ***These methods are not limited to photolithography.*** Once a positionally defined region of a substrate has been deprotected, polypeptide synthesis occurs essentially identically to synthesis of a single polypeptide on a solid substrate. Among other factors, the deprotection of the positionally defined area is crucial to the instantly claimed methods, so that one or more amino acids are added to a nascent polypeptide in only the desired regions of the substrate.

Thus, one skilled in the art would be able to combine the instant teachings on deprotection methods at positionally defined locations with a previous knowledge of how to synthesize a polypeptide, in order to prepare an array of polypeptides at positionally defined locations on a substrate. Contrary to the Examiner's assertion, there is no need for the Applicants to specifically exemplify how one skilled in the art would perform each of the deprotection methods disclosed in the instant specification when those methods are already known and can be readily applied to the instantly claimed methods. Furthermore, Applicants are not required to teach *every possible* method of deprotecting or activating a functional group in a positionally defined region. Applicants have taught a sufficient number of deprotection methods to enable one skilled in the art to select from a variety of methods of deprotecting functional groups in a positionally defined region. Moreover, the instant teachings, in combination with the teachings on deprotection methods and synthesis of a *single* polypeptide chain in the prior art

enable one skilled in the art to practice the full scope of the instant claims. Reconsideration and withdrawal of the rejection are respectfully requested.

Rejection of Claims 172-184, 186 and 188-192 Under 35 U.S.C. § 112, First Paragraph (Written Description)

Claims 172-184, 186 and 188-192 are rejected under 35 U.S.C. § 112, first paragraph, as containing subject matter which was not described in the specification in such a way as to reasonably convey to one skilled in the art that the inventors had possession of the claimed invention. In the Office Action mailed December 18, 2001, the Examiner states that a representative sample of methods of making the compounds and/or a showing of sufficient identifying characteristics is required to demonstrate possession of the claimed generics. The Examiner also states that the specification description is directed to the use of photolithographic techniques in the methods of making arrays of chemical compounds, and the Examiner concludes that the photolithographic techniques do not provide an adequate representation regarding the open-ended method of synthesizing a polypeptide array of the instant claims.

Applicants respectfully disagree with the Examiner's characterization of the specification. While the specification certainly fully describes the use of photolithographic techniques in the instantly claimed method, the use of numerous other techniques are disclosed in the specification. A listing of activating agents (which achieve deprotection of a functional group) can be found at page 19, line 38 through page 20, line 6, page 21, lines 7-28, page 63, line 33 through page 64, line 6, and page 133, lines 26-38 of the specification. Such activating agents or deprotection methods include electron beam irradiation, x-ray irradiation, electric current, electric field, magnetic fields, chemical agents, heat, laser pumping and oxidation and reduction with microelectrodes. These activating agents represent an extensive description of various techniques one can use to carry out the claimed method.

There is no need to describe the techniques in further detail, because they were known as of the earliest effective filing date of the invention, and "what is conventional or well known to one of ordinary skill in the art need not be disclosed in detail" (MPEP 2163). Moreover, means of using these techniques selectively (i.e., within a positionally defined region) were known as of the earliest effective filing date, so that again adequate written description of the invention is

fulfilled by simply naming that technique. In other words, the instant application provides a template method in which the use of one known activating agent in selectively preparing the invention is disclosed and the other activating agents are simply listed, because the manner of using them was already well known and described in the art. This is analogous to *Rasmussen*, described in MPEP 2163:

> See, e.g., *Rasmussen*, 605 F.2d at 1214, 211 USPQ at 326-27 (disclosure of a single method of adhering applying one layer to another was sufficient to support a generic claim to "adheringly applying" because one skilled in the art reading the specification would understand that it is unimportant how the layers are adhered, so long as they are adhered)

Similarly, the way a positionally defined region is selectively activated in the instant claims is unimportant, so long as it selectively activated. Thus, the invention of the instant claims is adequately described to support the claimed genus. Reconsideration and withdrawal of the rejection are respectfully requested.

CONCLUSION

In view of the above remarks, it is believed that all claims are in condition for allowance, and it is respectfully requested that the application be passed to issue. If the Examiner feels that a telephone conference would expedite prosecution of this case, the Examiner is invited to call the undersigned at (978) 341-0036.

Respectfully submitted,

HAMILTON, BROOK, SMITH & REYNOLDS, P.C.

By Jesse A. Fecker

Jesse A. Fecker, Ph.D.
Registration No.: 52,883
Telephone: (978) 341-0036
Facsimile: (978) 341-0136

Concord, MA 01742-9133
Dated: 4-25-03

EXHIBIT D

CHAPTER 4

LITHOGRAPHY

R. K. WATTS

4.1 INTRODUCTION

A lithograph, for people interested in art, is a less expensive picture made by impressing in turn several flat, embossed slabs, each covered with greasy ink of a particular color, onto a piece of stout paper. The various colors or levels must be accurately aligned, or registered, with respect to one another within some registration tolerance to produce the effect intended by the artist who carved or etched the slabs. Many "originals" can be made from the same slabs as long as the yield (ratio of good pictures to the total) remains adequately high. The technique was first used in the late eighteenth century, but was perhaps suggested by scenes carved in bas relief on more or less flat stones by many ancient peoples. For centuries it has been common practice for scholars and art lovers to copy these scenes by pressing a paper onto the relief to transfer the image to the paper.

Figure 1 illustrates schematically the lithographic process used to fabricate circuit chips. The exposing radiation is transmitted through the "clear" parts of a mask. The circuit pattern of opaque chromium blocks some of the radiation. This type of chromium/glass mask is used with ultraviolet (UV) light. Other types of exposing radiation are electrons, x-rays, or ions. Shadow (proximity) printing may be employed where the gap between mask and wafer is small. In the case of a nonexistent gap, the method is called contact printing. Or some sort of image-forming system (a lens, for example) may be interposed between mask and wafer.

Therefore, lithography for integrated circuit manufacturing is analogous to the lithography of the art world. The artist corresponds to the circuit designer. The slabs are masks for the various circuit levels. The press corresponds to the exposure system, which not only exposes each level but also aligns it to

EXHIBIT
tabbies
D

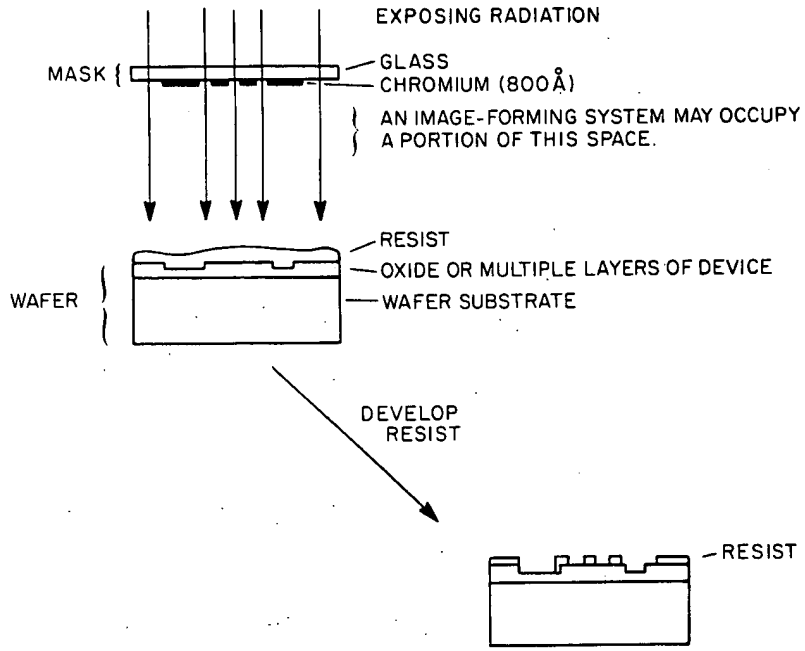

FIGURE 1
Device lithography generalization.

a completed level. The ink may be compared either with the exposing radiation or with the radiation-sensitive resist. And the paper can represent the wafer into which the patterns will be etched, using the resist as a stencil.

Optical lithography has penetrated the "1 μm barrier" of resolution. As other lithographic techniques such as those using electron, x-ray, or ion radiation have improved, so has optical lithography. For these competing methods large teams of capable people have been working steadily for ten years or more. Several methods have only one or two key problems remaining to be solved. Solution generally requires application of standard, but difficult and meticulous, engineering.

4.2 OPTICAL LITHOGRAPHY

Optical lithography comprises the formation of images with visible or ultraviolet radiation in a photoresist using contact, proximity, or projection printing (discussed in Section 4.2.3). For integrated circuit production the linewidth limit of optical lithography lies near 0.4 μm, although 0.2 μm features may eventually be printed under carefully controlled conditions. Optical lithography will continue to occupy the primary position for the foreseeable future.

4.2.1 Optical Resists

Photoresists are of two types. A negative resist on exposure to light becomes less soluble in a developer solution, while a positive resist becomes more soluble. Commercial negative resists, such as Kodak Microneg 747, consist of two parts: a chemically inert polyisoprene rubber, which is the film-forming component, and a photoactive agent. The photoactive agent on exposure to light reacts with

the rubber to form crosslinks between rubber molecules, making the rubber less soluble in an organic developer solvent. The reactive species formed during the exposure can react with oxygen and be rendered ineffective for crosslinking. Therefore the resist is usually exposed in a nitrogen atmosphere.

The developer solvent dissolves the unexposed resist. The exposed resist swells as the uncrosslinked molecules are dissolved. The swelling distorts the pattern features and limits resolution to 2 to 3 times the initial film thickness.

Positive resists have two components: a resin and a photoactive compound dissolved in a solvent. The photoactive compound is a dissolution inhibitor. When it is destroyed by exposure to light, the resin becomes more soluble in an aqueous developer solution. The unexposed regions do not swell much in the developer solution, so higher resolution is possible with positive resists. The development process of projection printed images in positive resists has been modeled theoretically.[1] It is an isotropic etching process. The sensitivity of most standard resists peaks in the 300 to 400 nm spectral range. Two examples of commercially available positive resists are MP-2400 and HPR-206.

The light intensity $I(\lambda, z)$ which is effective in exposing a volume element of resist at height z above the substrate depends on the reflectivity of the substrate, the thickness T of the resist ($T > z$), and the convolution of the absorption spectrum of the resist with the spectrum of the incident light. The refractive index of most resists is about 1.6, leading to an optical mismatch at the air/resist interface. If the substrate is highly reflective, the interference pattern of standing waves that are set up has a node at the substrate and a peak amplitude that depends on resist thickness T. Figure 2 shows the standing waves. This variation in peak intensity with resist thickness becomes less with decreasing substrate reflectivity and increasing absorption by the resist. Since resist thickness varies at a step in substrate topology, the resulting difference in effective exposure leads to size variations in the resist image. Because of the high resolution of positive resists, the standing wave patterns are often well resolved, and the resulting corrugations are seen in the resist edge profile.

Photoresists are being developed for exposure at shorter wavelengths where higher resolution is possible. A few such deep UV resists are poly-methyl methacrylate (PMMA), sensitive for $\lambda < 250$ nm; polybutene sulfone, sensitive for $\lambda \leq 200$ nm; and MP-2400, sensitive for $\lambda = 250$ nm. At these shorter wavelengths, the radiation quantum is large enough to produce scission (breakage) of the molecular chain.

Other properties of resists that are quite important are good adhesion to the substrate and resistance to wet and dry etch processes. In general, the commercially available optical resists are compatible with such processes.

The unwanted variation of feature size in the resist image is due to many effects, some related to resist properties and resist processing and others to the exposure tool. Variation in feature size can be minimized by proper control of exposure and development.

Computer modeling of resist images is an important field of study. For an introduction to this subject, see Chapter 10 of this book and Chapters 2 and 4 of Reference 2.

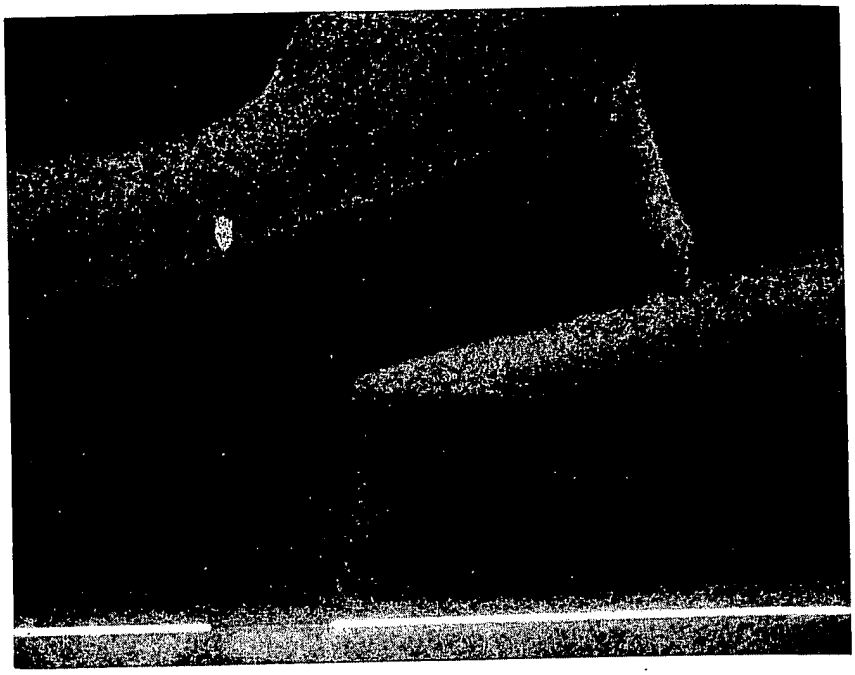

FIGURE 2
Standing waves in resist profile.

4.2.2 Contact and Proximity Printing

In contact printing a photomask is pressed against the resist-covered wafer with pressures typically in the range of 0.05 atm to 0.3 atm and exposured by light of wavelength near 400 nm. Very high resolution (≤ 1 μm linewidth) is possible, but because of spatial nonuniformity of the contact, resolution may vary considerably across the wafer. To provide better contact over the whole wafer, a thin (0.2 mm) flexible mask has been used; 0.4 μm lines have been formed in a 0.98 μm resist.[3] The contact produces defects in both the mask and the wafer so that the mask, whether thick or thin, may have to be discarded after a short period of use. For example, one worker reports mask defect densities increasing to 37 defects/cm^2 after 15 exposures from 13 defects/cm^2 after 5 exposures.[4] Defects include pinholes in the chromium film, scratches, intrusions, and star fractures.

Contact printing nevertheless continues to be widely used. Features as small as 0.25 μm have been produced in 1.8 μm thick PMMA resist using 200 to 260 nm radiation.[5] Quartz or Al_2O_3 mask substrates must be used to pass these shorter wavelengths, since the usual borosilicate glass strongly absorbs wavelengths less than 300 nm.

Proximity printing has the advantage of longer mask life because there is no contact between the mask and the wafer. Typical separations between mask and wafer are in the range of 20 to 50 μm. Resolution is not as good as in contact printing or projection printing.

Figure 3 shows proximity printing in the schematic form of a mask with a

long slit of width W separated from a parallel image plane (wafer) by a gap g. We assume that g and W are larger than the wavelength λ of the imaging light and that $\lambda << g < W^2/\lambda$—the region of Fresnel diffraction. Then the diffraction that forms the image of the slit is a function only of the particular combination of λ, W, and g which we shall call the parameter Q where

$$Q = W\sqrt{2(\lambda g)} \tag{1}$$

The diffraction patterns are well known. Some are shown in Fig. 4 for $Q = 2$, 3, and 7 (solid curves).[6] The limit $g < W^2/\lambda$ corresponds to $Q > \sqrt{2}$. The dashed rectangles in Fig. 4 show the light intensity at the mask. The larger the value of Q, the more faithful the image. Thus the resolution becomes better at smaller gaps and shorter wavelengths.

Two other noteworthy features of the diffraction patterns are the ragged peaks and the slope near $x = W/2$. The peaks can be smoothed by use of diverging rather than collimated light. The dotted curves are for light with a divergence half-angle $\alpha = 1.5\lambda/W$ radians. If α becomes large, the edge slope is reduced further, increasing linewidth control problems. Some smoothing also occurs because of the spread of wavelengths in the source, but this is a smaller effect. The illumination system must provide an apparent source size large enough to give a value of α—typically a few degrees—optimized for the smallest features to be printed. This is illustrated in Fig. 5. The mercury arc used as source is too small to yield the required α, so a scheme like that illustrated in Fig. 5c is used. The optical system must also minimize nonuniformity of intensity across the field; typically this may be 3 to 5%. Figure 6 shows the illumination system of a proximity printer. The illumination is telecentric, or normally incident, at the mask to prevent runout (magnification) errors. With a Hg arc source the strong lines at 436 nm, 405 nm,

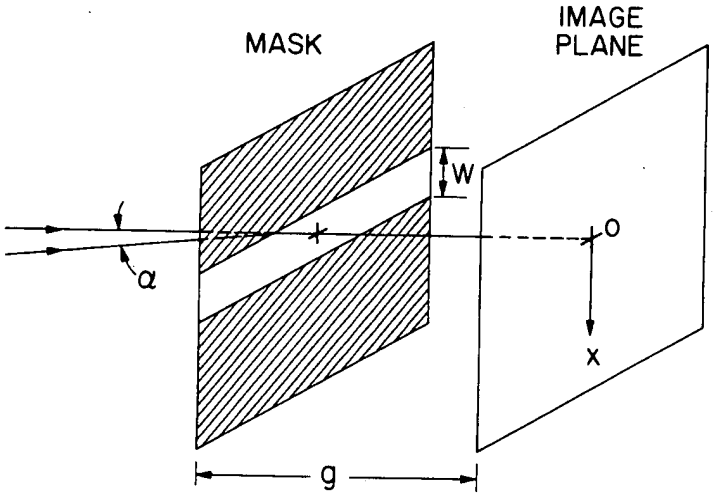

FIGURE 3
Proximity printing idealization.

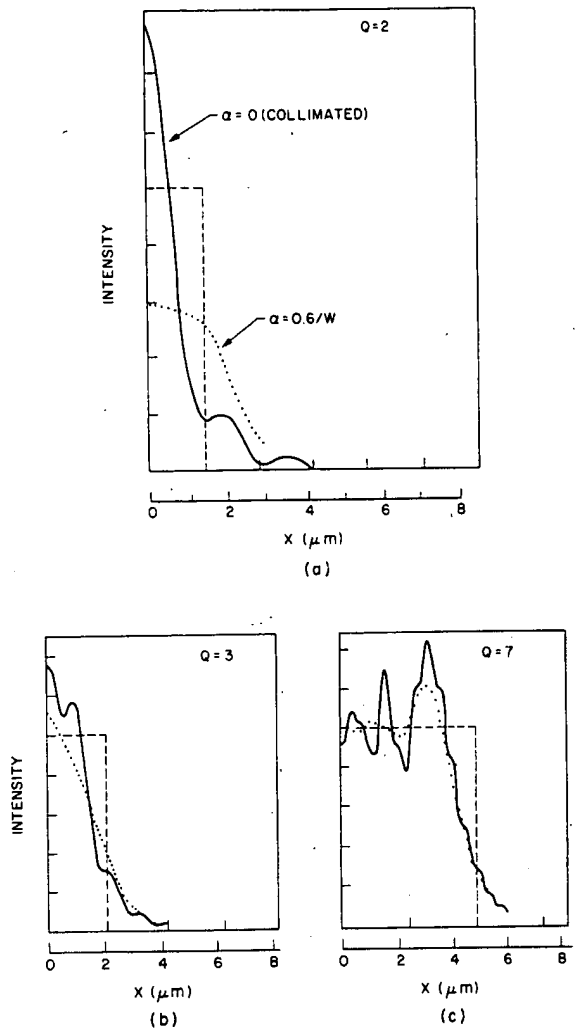

FIGURE 4
Image of slit with $Q = 2, Q = 3$, and $Q = 7.g = 10$ μm; $\lambda = 0.4$ μm. (*After Watts, Ref. 47.*)

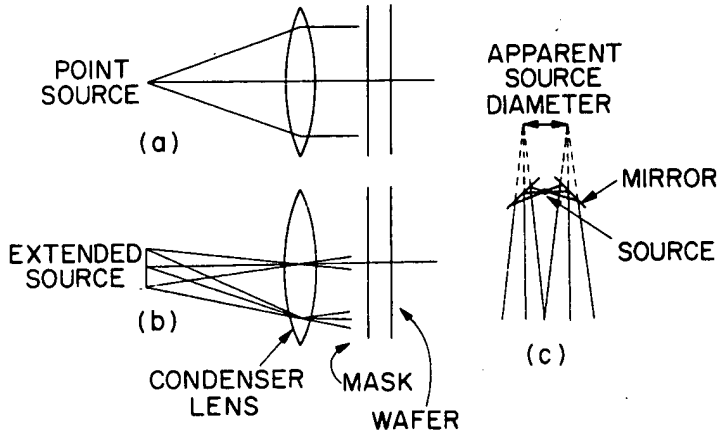

FIGURE 5
Proximity printing with collimated and uncollimated light. (*After Watts, Ref. 47.*) (a) shows a point source. (c) shows a way of obtaining an extended source like that depicted schematically in (b).

and 365 nm provide exposure flux. The same printer is available with Xe–Hg source for enhanced output in the 200–300 nm spectral region. Exposure times of 1 min (a very long exposure compared with standard resists) are required with PMMA resists, and 2 μm resolution is obtained with $g = 10$ μm to 20 μm.[7]

The edge of a feature in developed resist occurs at the position where the product of light intensity and exposure time equals the resist threshold dose. Linewidth control is in general more difficult in proximity printing than in contact printing. Linewidth is influenced by variations in light intensity, gap g, and resist properties. Linewidth has been measured as a function of light intensity I and mask-wafer gap.[8] The linewidth variation, defined as the printed width minus the width of the line on the mask, is proportional to ln I and to $\sqrt{g}$, and for each value of g there is an optimum exposure intensity which minimizes the effect of gap variation on linewidth. The mask-wafer gap can vary across a wafer and from one wafer to another because of wafer and mask bowing and dirt particles between the wafer and wafer chuck. This last problem is solved with a pin chuck, in which only a number of points contact the wafer. For exposure intensity near the optimum value, control of exposure to within 13% should provide linewidth control of ± 0.5 μm, even for large variations of the gap g. Linewidth control to within ± 0.25 μm with a 50 μm gap has been reported.[4]

Because of the sloping edges of the diffraction pattern of the slit, the image of a mask object consisting of equally spaced parallel lines will lose definition as the spacing between lines decreases and the edge tails begin to overlap. If I_M is the peak intensity in the image (on the lines) and I_m is the minimum intensity

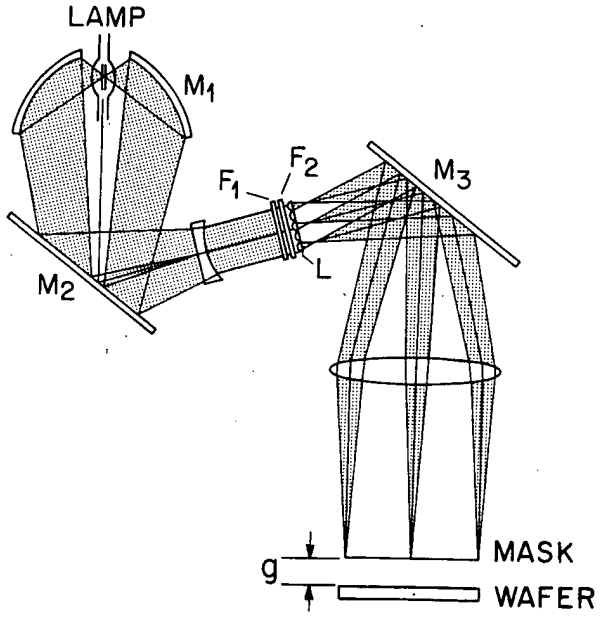

FIGURE 6
Illumination system of Canon PLA 500F proximity printer. F = filter. M = mirror. L = fly's eye lens. (*After Watts, Ref. 47.*)

in the image (between lines, where this quantity ideally should be zero), the modulation of the image M_i is given by

$$M_i \equiv \frac{I_M - I_m}{I_M + I_m} \tag{2}$$

M_i is a function of linewidth, line spacing, gap, and wavelength.[9] For proper exposure of resist, a ratio I_M/I_m of at least 4 is desirable. This corresponds to $M_i = 0.6$, a value which can be exceeded only with very small gaps. Further loss of modulation can be reduced by use of Fe_2O_3 or Cr_2O_3–Cr masks, which have much lower reflectivity than Cr and reduce scattered light under the opaque parts of the mask. (Cr_2O_3–Cr means that the chromium is covered with a thin chromium oxide layer to reduce reflectivity.)

4.2.3 Projection Printing

Projection printing offers higher resolution than proximity printing together with large separation between mask and wafer. Four important performance parameters of a printer are resolution, level-to-level alignment accuracy, throughput, and depth of focus. The resolution of an optical imaging system of numerical aperture $NA = \sin \alpha$ with light of wavelength λ is, according to Rayleigh's criterion, $0.61\lambda/\sin \alpha$—the separation of two barely resolved point sources.[10] The Rayleigh depth of focus[10] is given by $\pm \lambda/(2 \sin^2 \alpha)$. However, near the limiting resolution of the system, the contrast in the image is uselessly small. We shall see how optical performance can be specified in a more meaningful way by means of the system transfer function.

We consider a general optical system (Fig. 7) with no aberrations. An aberration is a departure of the imaging wavefront from the spherical form; that

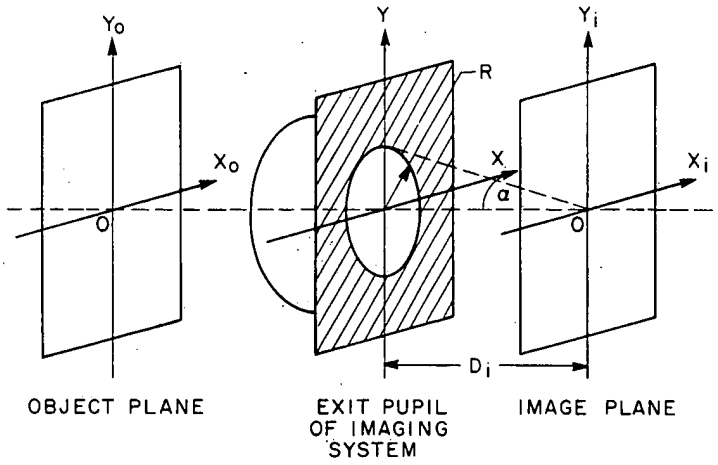

FIGURE 7
Projection printing idealization. (*After Watts, Ref. 47.*)

is, a spherical wave diverging from a point in the object plane is converted to a spherical wave converging to a point in the image plane. The f number of the system is $F \equiv D_i/2R$, and the numerical aperture is $NA = \sin \alpha = R/\sqrt{(D_i^2 + R^2)} \approx R/D_i$. R is the radius of the exit pupil, and D_i is the distance from this pupil to the image plane.

We want to recall briefly some results from the theory of image formation and to show how the transfer functions differ for coherent and incoherent imaging systems.[10] For coherent object illumination all points in the object have wave amplitudes with fixed phase relationships, and all phases have the same time dependence. For example, in Fig. 5a the phase varies across the mask plane at right in a way simply determined by the path lengths from the point source. On the other hand, if there is no phase correlation and the phases vary independently from point to point across the object, the illumination is spatially incoherent. This is the situation in Fig. 5b. We consider first the coherent case. It is not necessary that the radiation be monochromatic, only that the wavelength spread be small compared with the average wavelength. The wavelength λ can stand for the average wavelength.

The field amplitude at point x_i, y_i in the image plane (the wafer) will be called $U_i(x_i, y_i)$. It is caused by a field distribution $U_o(x_o, y_o)$ in the object plane (the mask). We define a pupil function $P(x, y)$ to represent the transmission of the round exit pupil, or hole, shown in Fig. 7. For points (x, y) within the pupil, $P = 1$; for points outside, $P = 0$. The simplest object is a point source at $x_o, y_o = 0$. The image of this source has the form

$$I_i(x_i, y_i) = \frac{\pi}{(2\lambda F)^2}[2J_1(s)/s]^2, s = \left(\frac{\pi}{\lambda F}\right)\sqrt{x_i^2 + y_i^2} \tag{3}$$

This is the well-known Airy pattern. J_1 is the first-order Bessel function. It is also called the point-spread function because the projection system spreads the point into the circular image represented by Eq. 3. The diameter (twice the distance from the origin to the first zero of J_1) of the pattern is 2.4 λF. Thus, the smaller the wavelength and the f number (or the larger the NA) of the projection system, the better the resolution.

High fidelity audio components are characterized in large part by the frequency response function. For a good loudspeaker the frequency response is flat over the whole audio range, dropping to zero near 20 Hz and 20 kHz. The frequency response function indicates how the speaker degrades the incoming signal, whose Fourier transform is a frequency spectrum. The output spectrum is obtained by multiplying each component of the input by the value of the frequency response function at that frequency. Similarly, optical systems are characterized by a frequency response function H, which is called in this case the optical transfer function. In optics the spatial frequency, or number of lines per mm in a grating pattern of equal lines and spaces, is the analog of temporal frequency, and a spatial coordinate, say x, is the analog of the time coordinate t. If $G_i(u, v)$ and $G_o(u, v)$ are the Fourier transforms of $U_i(x_i, y_i)$ and $U_o(x_o, y_o)$ respectively, then $H(u, v)$ is given by

$$G_i(u, v) = H(u, v)G_o(u, v) \tag{4}$$

Just as in the electrical case, the output (image) spectrum is obtained from H and the input (object) spectrum. It can be shown that

$$\begin{aligned} H(u, v) &= P(u\lambda D_i, v\lambda D_i) \\ &= 1, \quad \text{if } \sqrt{u^2 + v^2} \leq R/\lambda D_i \\ &= 0, \quad \text{if } \sqrt{u^2 + v^2} > R/\lambda D_i \end{aligned} \tag{5}$$

The transfer function is equal to the pupil function. It is plotted in Fig. 8, where the cutoff (spatial) frequency is written $u_m/2 = R/\lambda D_i = 1/2\lambda F$.

Now let us consider spatially incoherent illumination, in which the phases vary randomly across the mask. The frequency response function H can be defined by an equation like Eq. 4 relating Fourier transforms of image and object *intensities*. (The intensity I is the time average of the squared amplitude, $I = < UU^* >$.) In the incoherent case H is given by the overlap of two displaced pupil functions, as shown in Fig. 9. It can be calculated simply to be

$$|H(u)| = \frac{2}{\pi}[\cos^{-1}(u/u_m) - (u/u_m)\sqrt{1 - (u/u_m)^2}], \tag{6}$$

for $u \leq u_m$. The limiting spatial frequency is twice as great as for coherent illumination, but image contrast or modulation is less at the lower frequencies. The transfer function describes how the system degrades the image of a sinusoidal object grating. In general there is a reduction in modulation and a phase shift. The modulation transfer function (MTF) at frequency u is the ratio of image modulation (see Eq. 2.) to object modulation for an object grating of periodicity u^{-1}.

$$|H(u)| = M_i(u)/M_o(u) \tag{7}$$

The authors of Reference 11 describe MTF measurements for projection, prox-

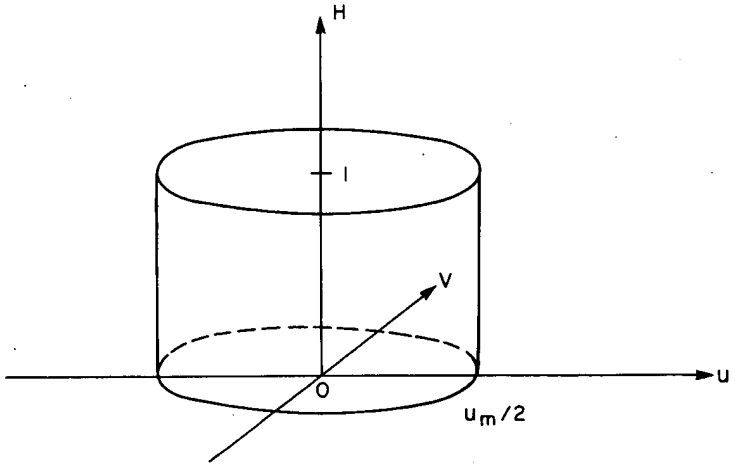

FIGURE 8
Coherent or optical transfer function for a round pupil.

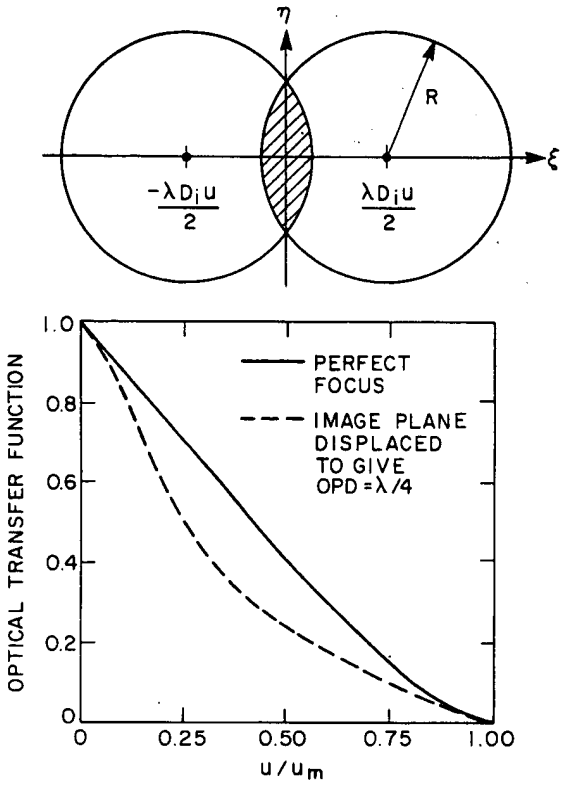

FIGURE 9
Incoherent transfer function for a round pupil, both in focus and out of focus.

imity, and contact printers using a square-wave bar target. The sine wave MTF can be calculated from the measured square-wave response.

In modern printers the illumination is intermediate between the coherent and the incoherent limits. The separation between points in the image which have correlated phases is neither infinite nor near zero. It can sometimes be varied by means of a diaphragm in the condenser illuminating the object. This is a familiar phenomenon to anyone who has used a microscope. As the aperture stop diaphragm is closed, the image looks "sharper," but interference rings appear around edges, and the light level drops. This is the near-coherent case. Opening the diaphragm causes the rings to disappear, and the image becomes brighter. The ratio S of the numerical aperture of the condenser to that of the projection optics is often used as a measure of coherence. (A slightly different definition is needed for the Kohler illumination often employed in printers.) $S = 0$ implies near coherence; if $S = 1$ the apertures are matched and the entrance pupil of the projection optics is filled to give nearly incoherent illumination. Further increase of S just causes more light scattering. Partial coherence has some advantages over incoherent illumination. The useful range, MTF > 0.6, is extended to higher spatial frequencies; edge gradients in the image become steeper; and the image is a little less sensitive to defocusing. Figure 10 shows a transfer function for a lens with $NA = 0.28$ and partial coherence $S = 0.75$ for the wavelength 436 nm. This is compared with a curve for a quartz lens with $NA = 0.38$ and incoherent

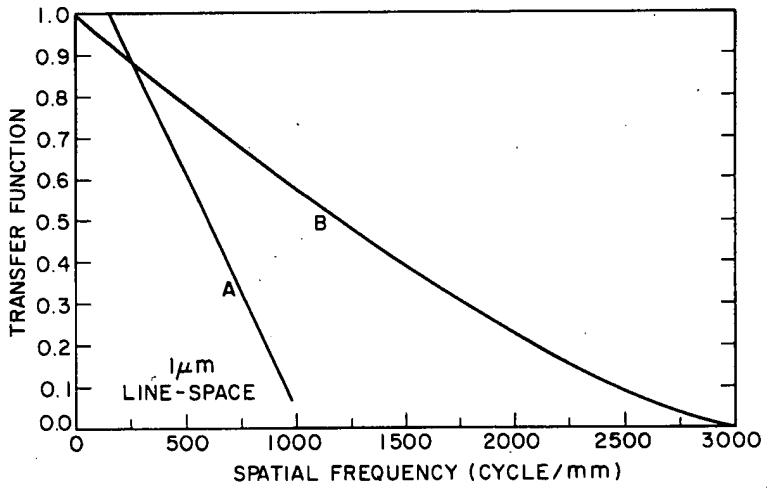

FIGURE 10
Comparison of two transfer functions. A. $NA = 0.28$; $S = 0.75$; $\lambda = 0.436$ μm. B. $NA = 0.38$; $S = 1$; $\lambda = 0.248$ μm.

illumination ($S = 1$). The wavelength is 248 nm. Obviously the second lens is capable of much higher resolution.

Since the transfer functions with round pupil are symmetrical under rotation about the vertical axis, they can be written and displayed as functions of a single variable u as in Eqs. 6 and 7 and Figs. 8 and 9. But it is understood that u stands for $\sqrt{u^2 + v^2}$. This two-dimensional nature explains why a small contact hole with predominant spatial frequency components $u = v = u_o$ requires a different exposure from a long line of the same width with $u = u_o$, $v \approx 0$, for $|H(\sqrt{2}u_o)|$ is less than $|H(u_o)|$. If both these types of features occur on the same mask, both types of resist image will not have correct dimensions. In general, for very small features representing high spatial frequencies, the required exposure depends on the shape of the feature and proximity to other features, setting a practical resolution limit much less than u_m.

Aberrations can be treated by including a phase error $\phi(x, y)$ in the pupil function: $P(x, y) \rightarrow P(x, y)\exp[i\,\phi(x, y)]$. This reduces the magnitude of the transfer function, except in the coherent case. Most printers have very nearly diffraction limited optics.

The focus error is a simple but important aberration. The error is a displacement of best focus away from its intended position. In Fig. 9 the dashed curve shows the effect of a displacement of the image plane or wafer from the focal plane by one Rayleigh unit $w = 2\lambda F^2$, corresponding to a phase error of $\pi/2$ at the edge of the pupil. Defocus affects different linewidths differently.[12,13]

Some information on several projection printers is collected in Table 1. They are of two types. The Perkin-Elmer 600HT uses reflective optics, as illustrated in Fig. 11. A curved lamp source (not shown) illuminates an arc on the mask, and this arc is imaged onto the wafer with unity magnification ($m = 1$). In this arrangement only a small zone of the spherical primary mirror is used, providing nearly diffraction-limited imaging. Mask and wafer are swept through the arc to

TABLE 1
Some projection printers

	m	NA	Field (mm^2)	$l_{0.6}$ (μm)	w (μm)	Align (3σ) (μm)	Throughput (wafers/hr)
Perkin Elmer 600HT	1	0.16	150ϕ	1.9	± 7.8	± 0.35	100
GCA 8000/1635	0.2	0.35	11 × 11	0.8	± 1.5	± 0.2	13(150mm)
GCA 8000/52529	0.2	0.29	18 × 18	1.1	± 2.6	± 0.2	37(150mm)
Nikon NSR 1505G4C	0.2	0.42	15 × 15	0.8	± 1.2	± 0.15	40(125mm)
Perkin Elmer SRA9535	0.2	0.35	17 × 17	0.9	± 1.7	± 0.15	50(125mm)
AT&T DUV	0.2	0.38	10 × 10	0.5	± 0.9	~± 0.3*	~30(100mm)

*2σ

form an image of the whole mask. The other printers use refractive optics: high quality lenses with many elements. They project a 5X reduced image onto the wafer.

As rough measures of resolution and depth of focus, $l_{0.6}$—the linewidth of the equal line/space pattern for which the MTF of an incoherent system would have a value 0.6—and w, the Rayleigh unit of defocus for an incoherent system, are listed in Table 1. Alignment tolerances and throughputs are those given by the manufacturer. If the whole image field cannot be filled with a large chip or several smaller ones and must be reduced in size, then more steps are needed to cover the wafer, and throughput decreases. The very small depth of focus of the high-resolution optics requires close automatic control of lens-to-wafer separation.

Because the size of the smallest feature resolvable with an optical system is proportional to $\lambda F, (u_m = 1/\lambda F)$, higher resolution is obtained by working at shorter wavelengths. There is more room for improvement here in projection printing than in proximity printing, with which resolution is proportional to $\lambda^{1/2}$. (See the discussion of proximity printing.) F can also be reduced, but useful field size decreases with decreasing F. In addition, depth of focus is proportional to λF^2. Thus it is better to reduce λ rather than F. The reduced depth of focus and degree of linewidth control accompanying higher resolution seem to represent an important practical limit. Some other problems encountered in the 200 to 300 nm

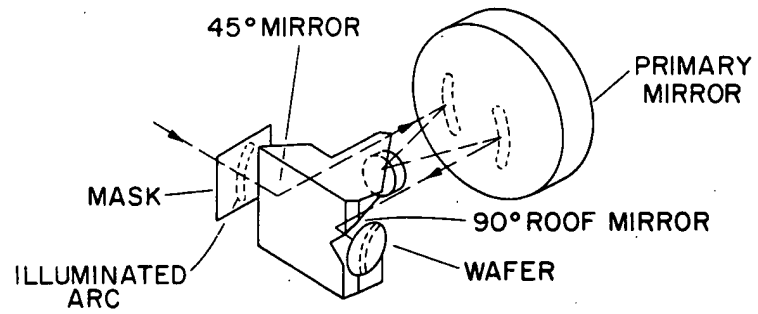

FIGURE 11
Projection optics, Perkin-Elmer printer.

wavelength range are increased Rayleigh scattering ($\sim \lambda^{-4}$), greater difficulty in reducing aberrations, and a need for new resists. Reflective optics are more suitable;[14] there are few optical glasses available for use in this wavelength range. Step-repeat exposure offers level-to-level registration precision that is independent of wafer size by separate alignment of each exposure field. The mask pattern dimensions are larger and therefore more convenient in the reduction projection systems than in those imaging with unity magnification.

The last entry in the table is an experimental stepper.[15] The source is an excimer laser operating at 248 nm. The lens is all silica. A next generation lens will provide the same resolution over a much larger field. Clearly this machine is a portent of things to come. The measure of resolution $l_{0.6}$ tabulated in Table 1 is meant to be an indication of the resolution obtained under production conditions. Ultimate resolution obtainable under carefully controlled conditions is higher. For example, the AT&T DUV stepper can image 0.35 μm line/space patterns in thin resist over a central part of the exposure field. More advanced systems will extend the ultimate resolution to about 0.2 μm.

Problem

Using the data of Table 1, divide field area by $l_{0.6}^2$ for each optical system shown. This ratio is the number of resolution elements. Explain why it is an order of magnitude larger for the first entry in the table than for the others despite the fact that *NA* is smaller for the first entry.

Solution

The whole field listed in the table for the first entry is not really comparable with the other smaller fields. The field considered for this purpose should be the (smaller) area of the arc-shaped image, which is scanned to fill a larger circular field.

Problem

1 A proximity printer operates with a 10 μm mask-wafer gap, and a wavelength of 430 nm. Another printer uses a 40 μm gap with wavelength 250 nm. Which offers higher resolution?

2 Why must the reticle (mask) used in a wafer stepper be completely free from defects? Why can some defects be tolerated in systems exposing the entire wafer at once?

Solution

1 $Q = W\sqrt{\frac{2}{\lambda g}}$.

A. $\lambda = 0.43\ \mu m$, $g = 10\ \mu m \rightarrow Q = 0.68\ W$

B. $\lambda = 0.25\ \mu m$, $g = 40\ \mu m \rightarrow Q = 0.45\ W$

Therefore **A** gives higher resolution.

2 If a reticle contains a defect, that defect will appear in every exposed field on the wafer. If the field contains a single chip and the defect is fatal, then every chip will be inoperative. A mask projected onto the whole wafer at once need not be entirely defect free; a single defect will affect only one chip in this case.

4.3 ELECTRON LITHOGRAPHY

Electron lithography offers higher resolution than optical lithography because of the small wavelength of the 10–50 keV electrons. The resolution of electron lithography systems is not limited by diffraction, but by electron scattering in the resist and by the various aberrations of the electron optics. Scanning electron-beam systems have been under development for two decades, and commercial systems are available. The EBES (electron beam exposure system) machine has proved to be the best photomask pattern generator. It is widely used in mask shops. Because of the serial nature of the pattern writing, throughput is much less than for optical systems. However, some special products such as microwave transistors have for many years been manufactured by direct wafer patterning. In the first application to low-volume integrated circuits, some levels were patterned optically and some by electron beam.[16]

4.3.1 Resists

Electron exposure of resists occurs through bond breaking (positive resist) or the formation of bonds or crosslinks between polymer chains (negative resist). The incident electrons have energies far greater than bond energies in the resist molecules, and so all these energies are effective. Both bond scission and bond formation occur simultaneously. Which predominates determines whether the resist is positive or negative.

In a negative resist, electron-beam-induced crosslinks between molecules make the polymer less soluble in the developer solution. One crosslink per molecule is sufficient to make the polymer insoluble. Resist sensitivity increases with increasing molecular weight. If the molecules are larger, then fewer crosslinks are required per unit volume for insolubility. The polymer molecules in the unexposed resist will have a distribution of lengths or molecular weights and thus a distribution of sensitivities to radiation. The narrower the distribution, the higher will be the contrast γ. The exposure dose q has units of charge deposited by the beam per unit area—C/cm^2. Figure 12 shows thickness remaining after development for COP negative resist. γ is the slope and is called the contrast.

In a positive resist the scission process predominates, the exposure leading to lower molecular weights and greater solubility. Again, high molecular weight and narrow distribution are advantageous.

Two factors are of major importance in limiting resist resolution: swelling of the resist in the developer (more important for negative resists) and electron scattering. Swelling of negative resists, whether optical, electron, or X-ray, has two deleterious effects. Two adjacent lines of resist may swell enough that they touch. On contracting in the rinse they may not completely separate, leaving a "bridge" here and there. Secondly, this expansion and contraction weakens adhesion of very small resist features to the substrate and can cause small undulations in narrow (0.5 μm) lines. Both problems become less severe as resist thickness is reduced.

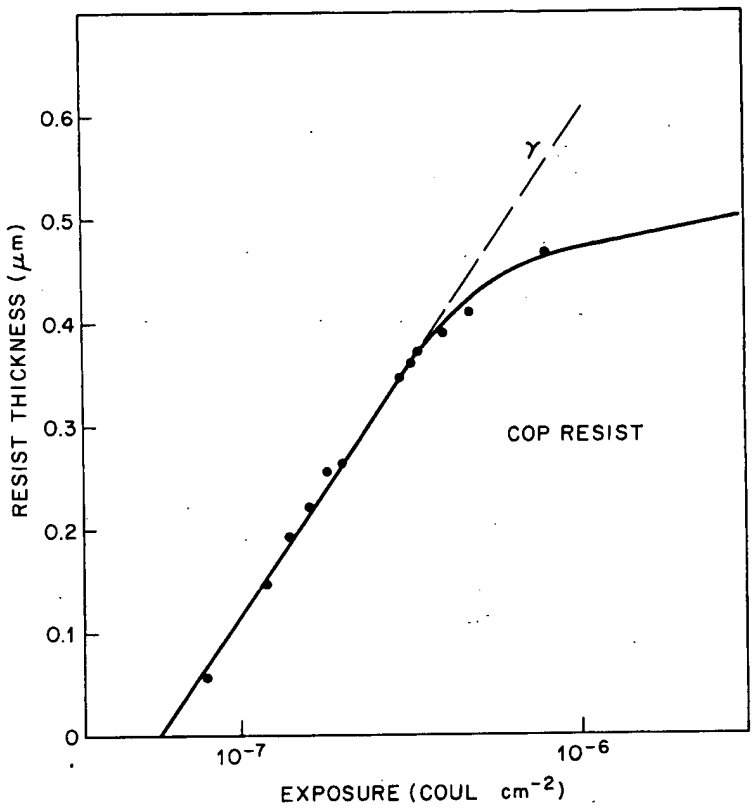

FIGURE 12
Exposure curve for COP negative resist.

When electrons are incident on a resist or other material, they enter the material and lose energy by scattering, thus producing secondary electrons and X-rays.[17] This fundamental process limits resolution of electron resist to an extent that depends on resist thickness, beam energy, and substrate composition. More electrons are scattered back into the resist from a GaAs substrate than from a silicon substrate, for example. The envelope of the electron cloud in the material can be pictured as an onion bulb pulled closer to the surface as beam voltage decreases. At higher beam voltage the electrons penetrate farther before being scattered over large lateral distances.

For an electron beam of zero width incident at position r on the resist-covered substrate, the distribution of energy deposited in the resist at depth z is closely approximated by

$$f(r,z) = a_1\exp[-r^2/\beta_f^2(z)] + a_2\exp[-r^2/\beta_b^2(z)] \qquad (8)$$

where $\beta_f(z)$ is the width of the forward-scattered beam in the resist, and $\beta_b(z)$ represents the back scattering from the substrate, with $\beta_b(z) >> \beta_f(z)$. $f(r,z)$ is the point-spread function, like that of Eq. 3 for optics. Generally the value of z of interest is that corresponding to the resist/substrate interface z_i. For a 25 keV electron beam penetrating 0.5 μm thick resist on a silicon substrate, for example,

$\beta_f(z_i) = 0.06\ \mu m$, $\beta_b(z_i) = 2.6\ \mu m$, and $a_2/a_1 = 2.7 \times 10^{-4}$. As separation between lines decreases, the back-scattered electrons contribute a greater dose between the lines where the dose should be zero. This is somewhat similar to the reduced modulation in an optical image at higher spatial frequencies. Indeed, electron exposure of resist may be treated by introducing a modulation transfer function, as in light optics. This formalism can also be applied to other types of lithography.

An exposed pattern element adjacent to another element receives exposure not only from the incident electron beam but also from scattered electrons from the adjacent element. This is called the proximity effect and is, of course, more pronounced the smaller the space between pattern elements. For example, an isolated 0.5 μm line requires 20–30% more exposure than 0.5 μm lines separated from each other by 0.5 μm. Thus, as pattern density increases, it becomes necessary to adjust exposure for various classes of elements, or in the extreme case, for different parts of elements.

Resist resolution is better in thinner resist layers. Minimum thickness is set by the need to keep defect density sufficiently low and by resistance to etching in device processing. For photomasks where the surface is flat and only a thin layer of chrome must be etched with a liquid etchant, resist thicknesses in the range 0.2–0.4 μm are used. For device processing in which topographic steps must be covered and more severe dry gas plasma etching is used, thicknesses of 0.5 μm to 2 μm are required. Most electron resists are not as resistant to dry etching as optical resists. One way of alleviating the problems of proximity effect, step coverage, and process worthiness is through use of a multilayer resist structure in which the thick bottom layer consists of a process-resistant polymer. In one realization of a three-layer structure, the uppermost layer of electron resist is used to pattern a thin intermediate layer, such as 1200 Å of SiO_2, which serves as a mask for etching the thick polymer below.[18] For electron lithography a conducting layer can be substituted for the SiO_2 to prevent charge buildup that can lead to beam placement errors. In another two-layer resist structure, both the thin upper layer and the thick lower layer are positive electron resists, but they are developed in different solvents. The thick layer can be overdeveloped to provide the undercut profile that is ideal for lift-off processing.

Table 2 lists a few readily available electron resists.[17] Many other resists are under development. PMMA stands for polymethyl methacrylate, the highest resolution resist known. MP-2400 is an example of an optical resist that is also electron sensitive. Values for sensitivity and resolution are approximate. Because faster electrons penetrate more deeply, more current is required at higher voltages. A resist is about one-half as sensitive for 20 keV electrons as it is for 10 keV electrons.

4.3.2 Mask Generation

The first widespread use of electron-beam pattern generators has been in photomask making. Let us see what advantages they have in this application. Figure

TABLE 2
Some electron resists

Resist	Polarity	Sensitivity (C/cm^2) @ 20 kV	Resolution (μm)	γ
PBS (Mead Tech.)	+	1.8×10^{-6}	0.5	1.7
PMMA (KTI Chem.)	+	1×10^{-4}	<0.1	2
EBR-9 (Toray Ind.)	+	1.2×10^{-6}	0.5	3
FBM-110 (Daikin Ind.)	+	1.5×10^{-6}	1.5	5
AZ 2400 (Shipley Co.)	+	2×10^{-4}	0.5	2
COP (Mead Tech.)	−	5×10^{-7}	1.5	0.8
OEBR-100 (Tokyo Okha)	−	5×10^{-7}	1.5	0.8
SEL-N (Somar Ind.)	−	1×10^{-6}	1	0.6
GMCIA (AT & T)	−	7×10^{-6}	0.5	1.7
CMS (Toyo Soda)	−	2×10^{-6}	0.7	1.5
RE-4000 N (Hitachi Chem.)	−	3.5×10^{-6}	1	1.3

13 shows two methods of making a photomask. On the left a reticle is patterned with an optical pattern generator—a machine which under computer control exposes and places pattern elements to form the chip image at 10× scale and which can make 60 to 100 exposures per minute. The pattern element is the image of an illuminated aperture of variable size. The reticle is then used as the object in a step-repeat camera, which steps the reduced image to fill the desired mask area. Stepping accuracy is interferometrically controlled. The master mask produced may be used in a projection printer or copied and the copies used in a contact printer. If an electron-beam pattern generator is used to make the reticle, the main advantage is speed in the case of complex chips. A large, dense chip can require 20 hours or more of optical pattern generator time, but only two hours or less of electron-beam pattern generator time.

On the right, Fig. 13 shows the more efficient method of electron-beam patterning. The mask may be either a 1× mask or a 5× or 10× reticle for use in

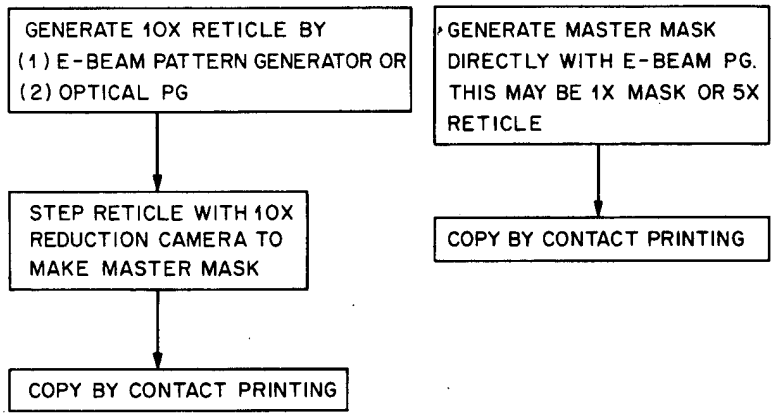

FIGURE 13
Two paths for generation of a photomask.

a wafer stepper. Table 3 shows some specifications of two types. CD stands for critical dimension.

Pattern placement errors (displacements of patterns from the desired locations on a mask) are measured with scanning, computer-controlled x–y optical measuring machines or with an electron-beam pattern generator. Figure 14 shows measurements at 100 points of a 100 mm × 100 mm array. For this mask maximum placement error was 0.099 μm. Stacking of two masks is often measured with an overlay comparator which superimposes the images of two masks. Fused silica mask substrates, with their low coefficient of thermal expansion, can reduce thermal contributions to stacking errors—the relative placement errors between two masks.

Misregistration of one circuit level to another on the wafer can be an important source of yield reduction. There are many contributions Δ_i to the total registration error Δ_t. If the contributions are mutually independent, then

$$\Delta_t = \left(\sum_i \Delta_i^2\right)^{1/2} \tag{9}$$

If the two masks used to image the level patterns do not overlay perfectly, there will be a registration error on the wafer. Thus the mask stacking errors contribute to Δ_t. The alignment tolerance of the printer that forms the image of the mask also makes a contribution. Another contribution to misregistration comes from wafer processing (etch tolerances, process-induced wafer distortion). If each of these three errors—mask stacking, alignment, and processing—has the small value 0.2 μm, then the total registration error would be $\Delta_t \geq 0.3$ μm. Since the ratio of minimum feature size to registration tolerance is usually in the range 3 to 5, registration of this precision would be barely adequate for circuits with 1 μm minimum features. There may be other contributions to Δ_t in addition to the three mentioned. For example, a change in the adjustment of the printer that transfers the mask image can lead to a change in image distortion with resulting placement errors.

Mask defects are either opaque spots in areas that should be transparent or pinholes where the chromium layer should be continuous. Sometimes critical masks are repaired to reduce the number of defects. Most vendors offer "zero

TABLE 3
Specifications of quartz master masks (Ultratech, Inc.), 125 mm plate, 100 mm array

	E-beam generated		Optically generated
	1X mask	5X reticle	1X mask
defects:	0.08/cm^2	0	0.03/cm^2
CD uniformity:	0.25μm*	0.25μm*	0.125μm*
CD tolerance:	±0.15μm*	±0.15μm*	±0.1μm*
stacking error:	±0.2μm*	±0.2μm*	±0.2μm*

*3σ

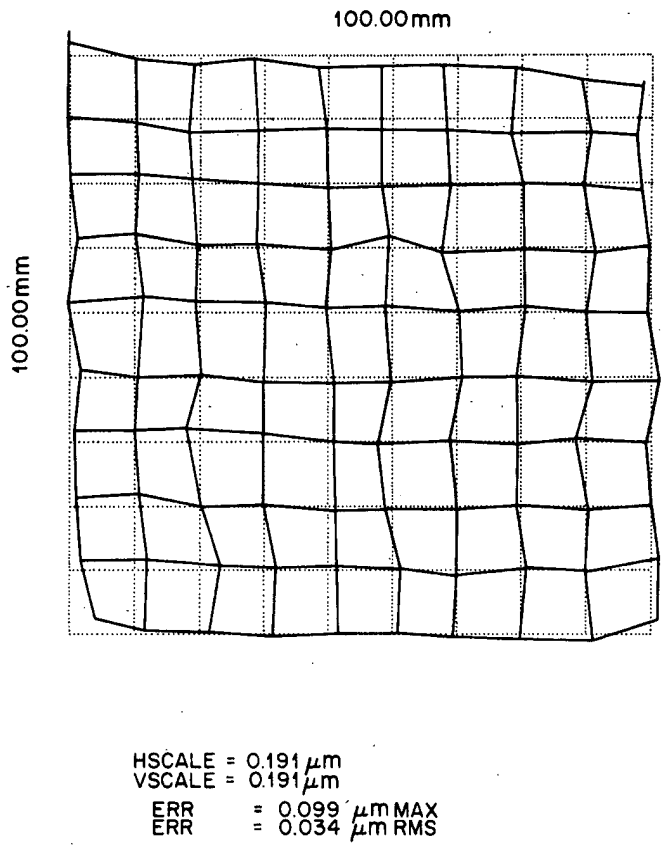

FIGURE 14
Photomask placement errors measured by MEBES at 100 points. The distortion scale is 0.191 μm per square.

defect" masks. If a master mask is copied by contact printing, the defect density of the copy will exceed that of the master. Defect density is generally measured by an optical instrument that compares one chip with a similar one on the mask and records differences or defects greater than a minimum size (~ 0.6 μm). Not every mask defect results in an inoperable chip. A reticle, however, must have no defects at all.

4.3.3 Electron Optics

Scanning electron-beam pattern generators are similar to scanning electron microscopes, from which they are derived. Figure 15 shows the basic probe-forming electron optical system. Two or more magnetic lenses form a demagnified image of the source on the wafer image plane. Provisions for scanning the image and blanking the beam are not included in the figure. The cathode is generally a thermionic emitter—either a tungsten hairpin or a pointed LaB_6 rod. Field emitters are also being used. In a field emitter, a strong electric field "pulls" the electrons out. The rod may be sintered material or a crystal. Emission current density from the cathode J_c is given by

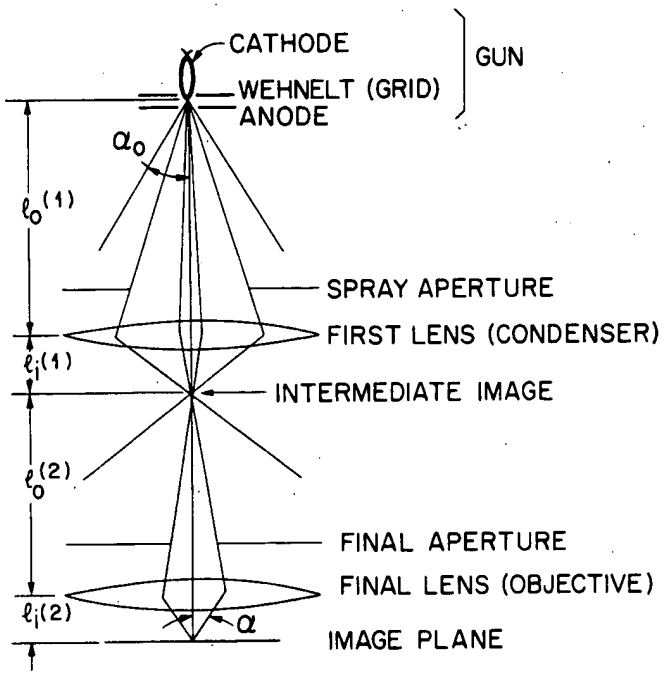

FIGURE 15
A simple two-lens probe-forming electron optical system.

$$J_c = AT^2\exp(-E_w/kT) \tag{10}$$

LaB_6 has a lower work function E_w than tungsten and about the same value of A (Table 4). A is called the Richardson constant and k is Boltzmann's constant. The electrons are accelerated through the voltage $V = 10$ to 50 kV and focused by the gun to a spot called the "crossover" of diameter $d_o = 10$ to 100 μm. The crossover is seen near the anode in Fig. 15. If I_b is the beam current at the crossover, the brightness—current density per unit solid angle—is

$$\beta = 4I_b/(\pi d_o \alpha_o)^2 \tag{11}$$

where d_o is as defined in Fig. 15. The maximum value of the brightness is

$$\beta = J_c e V/\pi kT \tag{12}$$

TABLE 4
Thermionic emitters

	E_w (eV)	A (A/cm^2-K^2)	T (K)	J_c (A/cm^2)
Sintered LaB_6	2.4	40	1923	65
LaB_6 xtl.<100>*	2.47	14	1923	17
W	4.5	60	2700	1.75

* Single crystal with <100> orientation.

The thermal field emission (TFE) source consists of a tungsten tip of radius 0.5 to 1 μm heated sufficiently (1100°C–1400°C) to provide annealing of sputtering damage. The TFE source permits relaxed vacuum requirements and better stability compared to a cold field emitter. Equation 11 does not apply and there is no gun crossover. The source, in this case, is a small (100–1000 Å) virtual one located inside the tip. Thus, the gun and the imaging optics are very different from those of the thermionic source we consider. Thermal field emitters are of interest because for small image spots they give higher currents than thermionic sources.

The lenses in the electron optical column (Fig. 15) are magnetic. The field of such a lens, $\vec{B} = \hat{e}_r B_r(r,z) + \hat{e}_z B_z(r,z)$, has cylindrical symmetry about the optical axis z. If a parallel beam of radius r_o enters the field of the lens, the electrons experience a force that causes those not on axis to rotate about the axis and turn toward it. For a thin lens the electron path beyond the lens is given by

$$dr/dz \approx -(r_o e/8mV)\int_{-\infty}^{\infty} B_z^2 dz \tag{13}$$

The constant $dr/dz = -r_o/f$, where f is the focal length of the lens and e is the electronic charge. Many rules of light optics apply here also, such as the thin-lens law relating object distance, image distance, and focal length:

$$1/l_o + 1/l_i = 1/f \tag{14}$$

The magnification of a lens is $M = l_i/l_o$. An intermediate image is formed by the first lens with magnification M_1, and this is the object which is further demagnified by the second lens to form a spot in the image plane of diameter

$$d_i = Md_o, \quad M = M_1 M_2 \tag{15}$$

where d_o is the object diameter and M_2 is the magnification of the second lens. Typically $M \approx 10^{-3}$–10^{-1}. Although the lengths $l_o^{(1)}$ and $l_i^{(2)}$ are fixed, $l_i^{(1)}$ and $l_o^{(2)}$ are variable. If current through the windings of the first lens of Fig. 15 is increased, $l_i^{(1)}$ decreases, M_1 is reduced, and the beam current passing through the final aperture is reduced because of the increased divergence of the beam at the intermediate image. The current density and current in the image plane are

$$J \leq \pi\beta\alpha^2 \quad \text{and} \quad I = J(\pi d_i^2/4) \tag{16}$$

Spot sizes of interest are in the range from 0.1 to 2 μm. This is far from the diffraction limit. From Section 4.2.3 the diameter of the central spot of the Airy pattern is $1.2\lambda/\alpha$. $NA(\simeq \sin\alpha)$ is the numerical aperture. For 15 keV electrons the wavelength $\lambda = 0.1$ Å. Taking $\alpha = 10^{-2}$ radians, we have a diffraction spot width

$$d_{diff} = 1.2\lambda/\alpha = 10^{-3}\,\mu\text{m} \tag{17}$$

Thus diffraction can be ignored. However, aberrations of the final lens and of the deflection system will increase the size of the spot and can change its shape as well. Aberrations of the other lenses are not so important since the intermediate images are larger. Figure 16 shows a typical double-deflection system above the

final lens, arranged so that the deflected beam always passes through the center of the lens. In some designs the deflected beam is incident normal to the wafer surface (telecentric) to minimize runout error for warped wafers. The deflection coils provide a magnetic field perpendicular to the beam axis. There will be another set of deflection coils to provide deflection perpendicular to the plane of the figure as well.

The aberrations are treated as independent contributions to spot broadening, each contributing a circle of confusion or a blur to the spot. The actual spot size in the presence of aberrations is then the square root of the sum of the squares of the independent contributions. The aberrations are of two types: aberrations of the undeflected beam and aberrations that are functions of the distance r in the image plane from the axis to the position of the deflected beam. The aberrations of the first type are

$$\text{Spherical aberration: } d_s = (1/2\,C_s)\alpha^3$$

$$\text{Chromatic aberration: } d_c = C_c(\Delta V/V)\alpha$$

Spherical aberration is the focusing of rays passing through different parts of the lens at different distances; a ray near the axis has a longer focal length than one farther from the axis. $e\Delta V$ is the spread of electron energies, usually a few eV. C_s and C_c are constants that characterize the aberrations. Astigmatism, a third type of aberration, results from the breaking of cylindrical symmetry in the column and can be removed by introducing compensating fields with stigmator coils (Fig. 16). Deflection aberrations, such as coma and field curvature, are proportional to $r^2\alpha$ or $r\alpha^2$. We lump them all together and call their contribution to the spot

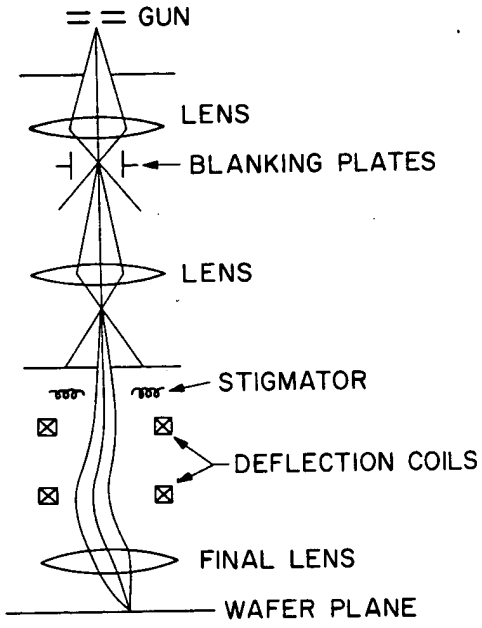

FIGURE 16
Electron optical system with double deflection.

spread d_{df}. In addition to the deflection aberrations, there is field distortion, but distortion is a shift of the image point, not a broadening of the spot. Table 5 shows these aberrations for the IBM VS1 machine.[19] We note that deflection aberrations dominate. Distortion and some of the deflection aberrations can be reduced by addition of correction signals to the deflection fields. Distortion with this machine is ± 2.5 μm at the edges of a 5 mm $\times$ 5 mm field, or $\pm 5 \times 10^{-4}$ expressed as a fraction of the field. For optical printers this ratio is typically much smaller.

Another source of spot broadening is the mutual Coulomb repulsion of the electrons as they traverse the column. For total column length L this contribution is approximately given by

$$d_{ee} \approx [LI/(\alpha V^{3/2})] \times 10^8 \mu\text{m} \tag{18}$$

This spreading becomes important only at large currents when small spot sizes or sharp edges of large spots are sought. For example, if $I = 500$ nA, $L = 70$ cm, $V = 20$ kV, and $\alpha = 10^{-2}$ rad, then Eq. 18 gives $d_{ee} = 0.12$ μm. Another effect of the interelectronic interactions is an increase of energy spread ΔV of the electrons. Through chromatic aberration of the optics, this leads also to broadening of the spot. In the presence of aberrations Eq. 16 becomes

$$I = (\pi^2/4)\beta\alpha^2[d^2 - d_s^2 - d_c^2 - d_{df}^2 - \ldots] \tag{19}$$

d is the beam diameter in the presence of aberrations,

$$d^2 = d_i^2 + d_s^2 + d_c^2 + d_{df}^2 + \ldots \tag{20}$$

Problem

An electron beam exposure system operates at 25 kV accelerating voltage. Column length is 1 m. Spot current is 300 nA, and numerical aperture of the final lens is 10^{-2} rad. The energy spread at the cathode is 0.2 V. If the coefficients of spherical and chromatic aberration are 10 cm and 62.5 cm respectively, what is the resolution limit at the center of the exposure field?

Solution

$$d_{ee} = (LI/\alpha V^{3/2}) \times 10^8$$

$$= 0.08\ \mu m$$

$$d_s = \frac{1}{2} C_s \alpha^3$$

$$= 0.05\ \mu m$$

$$d_c = C_c \left(\frac{\Delta V}{V}\right) \alpha$$

$$= 0.05\ \mu m$$

$$d = (d_{ee}^2 + d_s^2 + d_c^2)^{1/2} = 0.11\ \mu m$$

TABLE 5
Aberrations at the corners of 2 mm × 2 mm and 4 mm × 4 mm exposure fields for VS1.

	2 mm field	4 mm field
Spherical, d_s	0.01 μm	0.01 μm
Chromatic, d_c	0.04	0.04
Deflection, d_{df}	0.087	0.35
Total, no dynamic correction	0.095	0.35
Total, dynamic correction	0.043	0.050

4.3.4 Raster Scan and Vector Scan

In raster scan the beam is deflected repetitively over the exposure field, as in a television raster. The beam is turned on at various points in the scan to expose the desired pattern. The EBES machine, developed by Bell Laboratories and available commercially in the form of the MEBES system from Perkin Elmer, uses beam deflection in one dimension (mainly).[20] The writing scheme is shown in Fig. 17. The stage moves continuously in a direction perpendicular to the writing direction. The pattern data are decomposed into a number of stripes, and one stripe is written over all chips of the same type before the next stripe is begun.

The stripe is 2048 addresses wide, an address corresponding to a width from 0.1 to 1.0 μm. Beam diameter can be varied from 0.1 to 1.0 μm. The pattern

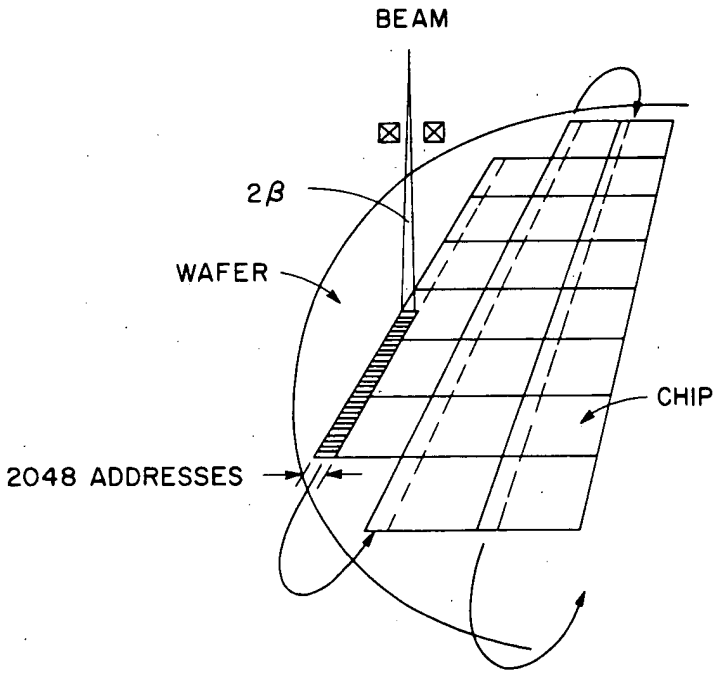

FIGURE 17
EBES / MEBES writing scheme. Curved arrows indicate the serpentine stage motion.

information comes to the blanking plates from a shift register at a 40 or 80 MHz rate. Since total time to write the 2048 scan is 31.6 μs − 12.5 ns per spot plus 6 μs for flyback, the writing rate is approximately 8 cm^2/min with a 0.5 μm address and 2.4 cm^2/min with 0.25 μm address.

In a vector-scan pattern generator the beam is directed sequentially to the parts of the chip pattern to be exposed. The pattern is decomposed into a number of elements (rectangles, triangles, etc.) and each one is filled in by the writing beam. Many vector-scan machines expose in step-repeat fashion. Figure 18 shows an exposure field of dimensions F × F. The alignment marks in the field corners are first scanned to set deflection amplitude, offset, rotation, and x–y scan axis orthogonality. Marks may be etched trenches in silicon, or they may be metal layers or other features that give sufficient contrast. A mark position is sensed by the change produced in the number of back-scattered and secondary electrons on scanning over the mark edges. Marks may be etched into a wafer and several circuit levels overlayed by reference to the marks. The accuracy of the overlay depends on many variables such as field size, alignment mark condition, resist thickness, and stability of field distortion from one level to the next. Reported values of overlay error lie in the range ±0.02 μm to ±0.6 μm. The beam is scanned over each pattern element in turn. Dotted lines indicate where the beam is turned off, that is, deflected by voltages applied to the blanking plates (Fig. 16) and prevented from passing through an aperture. For example, the rectangle shown might be specified in the program by an instruction such as

$$(x_1, y_1)\text{RECT}(x_2, y_2)\text{R}(\theta) \tag{21}$$

Software, as in optical pattern generators, consists of an operating system and a high-level system in which pattern elements and commands are simply expressed. In one such machine the point (x_1, y_1) is determined by 16-bit digital-to-analog

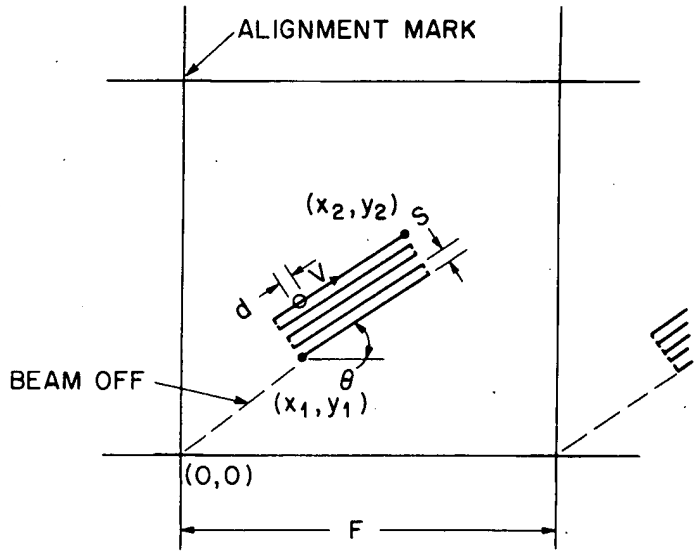

FIGURE 18
Vector scan writing of a rectangular pattern element. The scan starts at (x_1, y_1) and ends at (x_2, y_2).

converters, or DACs (65536 point resolution in x and y), and scan line lengths are determined by other DACs.

After all elements in the field are exposed, the stage is stepped to bring the next field under the beam and the exposure process is repeated. The stage need not provide highly precise motion. Stage position is generally monitored by a laser interferometer, and small differences from desired stage location are compensated by small offsets of the beam. If a chip is larger than an exposure field, then several fields can be used to expose the chip, but scan distortion at the field edges must be small enough so that patterns in adjacent fields are properly joined. If the machine is used to pattern masks rather than wafers, no alignment marks are used on the mask. In this case the deflection parameters are set by periodic reference to a mark fixed on the stage.

Once the beam current is set, exposure is controlled by varying the scan speed v and scan spacing s. These are set to the desired values for the whole pattern, or v might be set to different values for some pattern elements to compensate for proximity effects. From Eq. 21 it is obvious that few pieces of data are needed to trace out a pattern element that may contain very many beam diameters or "pixels." The proper exposure is found by exposing a test pattern at a series of scan speeds.

The scan field must be as large as allowed by deflection aberration and distortion because stage-stepping time affects throughput. Reported exposure fields lie in the range $F = 0.25$ mm to 6 mm—much smaller than for optical step-repeat machines.

Commercially available vector-scan machines are JEOL JBX6A3, EBMF of Cambridge Scientific Instruments, and Beamwriter of Philips. Vector-scan systems have also been developed by Hughes Research, IBM, AT&T, and Texas Instruments.

The EBES4 machine developed by AT&T Bell Laboratories has a continuously moving stage, unlike the step-repeat systems. Software is compatible with the other EBES/MEBES systems.[21] The coordinate system can be distorted digitally to correct for errors or to improve registration to existing levels. Column length was kept to 0.6 m to reduce Coulomb distortion of the spot (see Eq. 18). Three hierarchical deflection systems are used. Magnetic deflection provides coverage of a 0.28 mm square field with a 5 μs settling time. Deflection over a 32 μm square field is electrostatic with a 100 ns settling time. Microfigures are generated over a 2 μm square field by another set of electrostatic deflectors with settling time less than 0.5 ns. The combination of the three deflection systems is designed to be accurate to within $\pm$ 0.016 μm.

4.3.5 Variable Beam Shape

In the JEOL JBX6A3 machine shown schematically in Fig. 19, the spot is rectangular with variable size and shape. The image of the first square aperture may be shifted in two dimensions to cover various portions of the second aperture, which is the object imaged on the mask or wafer. Minimum rectangle width is 0.3 μm; maximum width is 12.5 μm. Maximum current density is 2A/cm^2

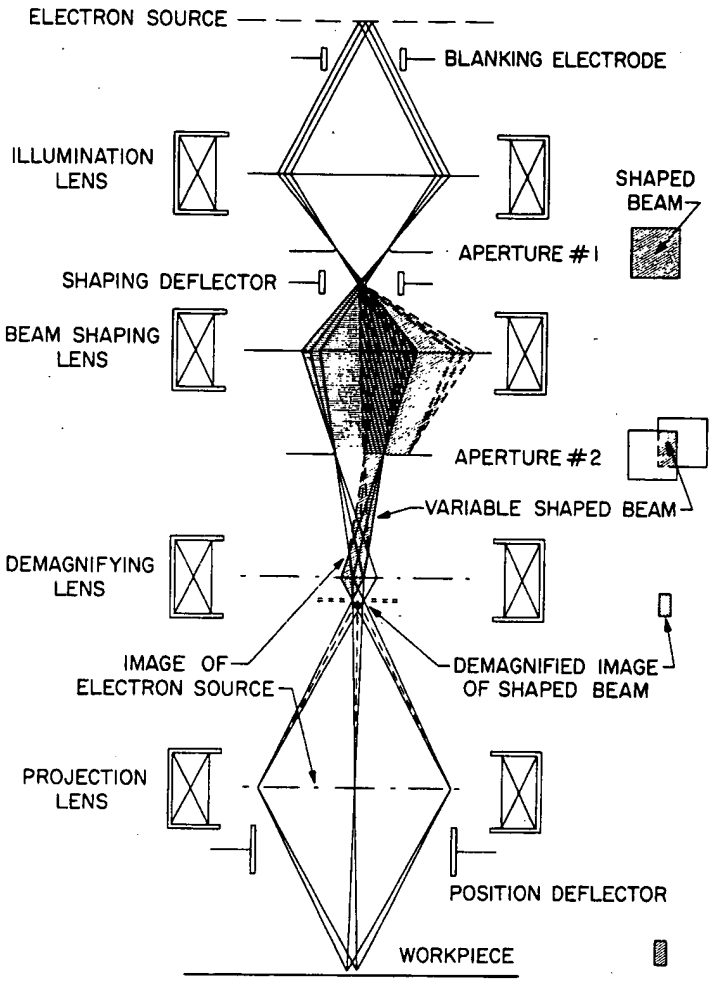

FIGURE 19
JEOL JBX6A3 electron optical system.

with the LaB_6 cathode. Electrostatic beam deflection is employed. Proximity effect corrections are easily made by variation of the exposure time of individual rectangles.. The maximum exposure field is 2.5 mm × 2.5 mm. Thus, many fields must be stepped to expose a mask or wafer. For a chip containing 9×10^4 rectangles the patterning time, assuming a time of 1.6 μs per shot, is 0.14 seconds. The time to step and align each exposure field, including a 0.25 s alignment time, is 0.39 seconds. Thus, for each chip containing four fields we have

$$t_e = 0.14 \text{ s}$$
$$t_{sr} = 1.56 \text{ s}$$
$$\overline{1.7 \text{ s}}$$

Total time to pattern a 100 mm wafer containing 282 chips would be 8.0 min. Thus, 7.5 wafers/hour could be patterned. Many wafers can be held at one time in the vacuum system so that the load/unload time for each wafer is small.

The shaped-beam methods offer a way to project many image points in parallel and to achieve faster exposure without the need for the fast deflection system required with a small scanned beam.[22] Design of any electron-beam pattern generator necessarily is based on many compromises. The designers of EBES4 first considered the variable-shaped-beam approach. However, the machine is intended for sub-0.75 μm patterns.

Problem

Some high-resolution photoresists are also good electron resists with $q \approx 20\mu$ C/cm^2. Suppose 20% of the chip area is scanned by the beam, that the field size is $F = 6$ mm, that the step-repeat and overhead times are $t_{sr} = 0.4$ s/field and $t_{oh} = 0.3$ s/field, and that there are $N = 190$ chips/wafer. Calculate throughput for $I = 10^2$ nA.

Solution

$$t = N(t_e + t_{sr} + t_{oh}). \quad t_e = \eta F^2 q / I.$$

$$\eta = 0.2, F = 0.6 \text{ cm}, N = 190, t_{sr} = 0.4 \text{ s}, t_{oh} = 0.3 \text{ s}.$$

$$t_e = (0.2)(0.6)^2(2 \times 10^{-5})(10^7)$$

$$= 0.144 \times 10^2.$$

$$t = (190)(14.4 + 0.4 + 0.3)$$

$$= 0.797 \text{ hr}.$$

$$t^{-1} = 1.26 \text{ wafers / hr}.$$

4.3.6 Electron Projection

Electron projection systems are another method of achieving high resolution over a large field with high throughput. Rather than a small beam writing the pattern in serial fashion, a large beam provides parallel exposure of a large area pattern.

In a 1:1 projection system parallel electric and magnetic fields image electrons onto the wafer. The "mask" is of quartz patterned with chrome and covered with CsI on the side facing the wafer. Photoelectrons are generated on the mask/-cathode by backside UV illumination. Westinghouse, Thomson CSF, Philips,[23] Toshiba, and Radiant Energy Systems have developed systems. The advantages of the system include stable mask, good resolution, fast step-repeat exposure with low sensitivity electron resists, large field, and fast alignment. Proximity effects can be compensated for by undersizing or oversizing the features on the mask. Or the electron energy can be increased to 50 keV or more. Apparently neither method is entirely satisfactory.

Another problem remains to be solved before this system can become a strong contender for the high-volume production of advanced chips. The cathode has an unacceptably short life, only 50 exposures, before the CsI must be replenished by evaporation of fresh material.

4.3.7 Electron Proximity Printing

An electron proximity printing system has been under development for a number of years by IBM Deutschland.[24] This is a step-repeat system in which a silicon membrane stencil mask containing one chip pattern is shadow printed onto the wafer. Since the mask cannot accommodate re-entrant geometries (doughnut, for example), these are printed with two masks. Registration is accomplished by reference to alignment marks on each chip. Overlay error is less than 0.05 μm (3σ). An advantage of this system is its ability to measure and compensate for mask distortions. Proximity effects must be treated by changing the size of pattern elements. The major disadvantage of the system is the need for two masks for each pattern.

4.4 X-RAY LITHOGRAPHY

Since the proposal for X-ray lithography in 1972, the technique has been under development in many laboratories.[25] We saw how diffraction effects are reduced and resolution improved by reducing the wavelength in optical lithography. If the wavelength is reduced further, all optical materials become opaque because of the fundamental absorption, but transmission increases again in the X-ray region. In X-ray lithography an X-ray source illuminates a mask, which casts shadows into a resist-covered wafer. Materials useful for the absorptive and transmissive parts of the mask, the atmosphere in the exposure chamber, and the resist are in large part determined by the absorption spectra of these materials in the X-ray region.

The X-ray absorption of several materials is shown in Fig. 20. Over wide ranges of wavelength the absorption coefficient of an elemental material of density ρ and atomic number Z is proportional to $\rho Z^4 \lambda^3$. As λ increases, the proportionality constant decreases in step-function fashion at the "absorption-edge" wavelengths corresponding to the ionization energies of the inner electrons of the K, L, and other shells. Note the large differences in the absorption coefficient observed for different materials at the same wavelength.

4.4.1 Resists

An electron resist is also an X-ray resist, since an X-ray resist is exposed largely by the photoelectrons produced during X-ray absorption. The energies of these photoelectrons are much smaller (0.3 keV to 3 keV) than the 10 keV to 50 keV energies used in electron lithography, making proximity effects negligible in the X-ray case and promising higher ultimate resolution.

On traversing a path of length z in resist or any other material an X-ray flux is attenuated by the factor $\exp(-\alpha z)$. For most polymer resists containing only H, C, and O and with density $\rho \approx 1$ gm/cm^3, a 1 μm thick resist film absorbs about 10% of the incident X-ray flux at the $\mathrm{Al}_{K\alpha}$ X-ray wavelength $\lambda = 8.3$Å. This small absorption has the advantage of providing uniform exposure throughout the resist thickness z and the disadvantage of reduced sensitivity. As in the optical case, X-ray resist sensitivity is generally quoted in terms of incident dose q(J/cm^2) required for exposure; sometimes absorbed dose αq(J /cm^3) is used.

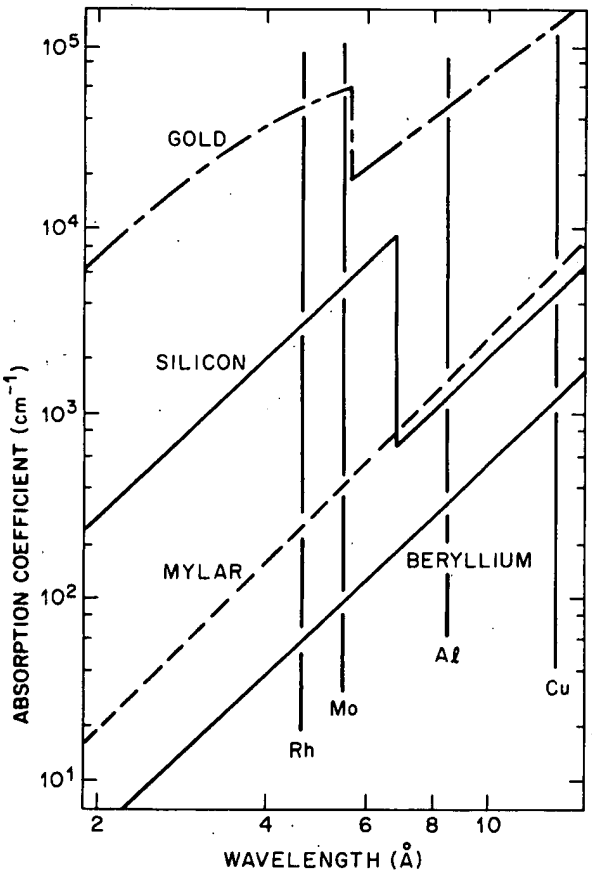

FIGURE 20
Absorption coefficients of several materials in the soft X-ray region. Sharp lines in the spectra of four sources (Rh, Mo, Al, Cu) are indicated.

For the shorter X-ray wavelengths the λ^3 dependence of the absorption coefficient leads to low sensitivity. This can be offset by incorporating heavier elements to increase absorption. For $Pd_{L\alpha}$ radiation, $\lambda = 4.37$ Å, the DCOPA resist incorporates chlorine. The Cl_K absorption edge at 4.40 Å provides higher absorption, and chlorine is a chemically reactive species. Thus, two effects contribute to higher sensitivity.

The negative resists are limited in resolution by swelling during development, as in optical and electron lithography. Thus, minimum features of only 0.75 μm can be resolved in DCOPA of final thickness 0.5 μm. Improved resolution can be obtained using thinner resist in a multilayer structure as in optical and electron lithography. Conventional X-ray sources produce flux at the wafer that is typically less than that available in optical lithography by a factor of $\sim 10^3$. Resist sensitivity must be $\lesssim 10$ mJ/cm^2 to prevent long exposure times.

4.4.2 Proximity Printing

Because the X-ray wavelength is small, diffraction effects can be largely ignored and simple geometrical considerations can be used in relating the image to the

pattern on the mask. The opaque parts of the mask cast shadows onto the wafer below. The edge of the shadow is not absolutely sharp because of the finite extent of the X-ray source (diameter of the focal spot of the electrons on the anode) at distance D from the mask. If the gap between mask and wafer, as shown in Fig. 21, is called g, this blur δ is given by

$$\delta = Sg/D. \tag{22}$$

Typical values are $g = 20\ \mu$m, $S = 3$ mm, $D = 40$ cm, $\delta = 0.15\ \mu$m. Resolution is determined by δ, by the minimum linewidth achievable in mask fabrication, and by properties of the resist used.

The angle of incidence of the X-rays on the wafer varies from 90° at the center of the wafer to $\tan^{-1}(D/R)$ at the edge of the exposure field of radius R. The shadows are slightly longer at the edge by the amount

$$\Delta = g(R/D). \tag{23}$$

This small magnification is generally of no concern. In the special cases where it may be undesirable, it can be compensated for when the mask is patterned. For multilevel devices the magnification must have the same value for each level, or at least its variation must be within the registration tolerance. This implies stringent control of the gap g. Wafer warping in processing depends on wafer thickness and orientation and on the nature of the process; it can be nearly eliminated with a proper vacuum chuck. It is not necessary that the gap have the same value at

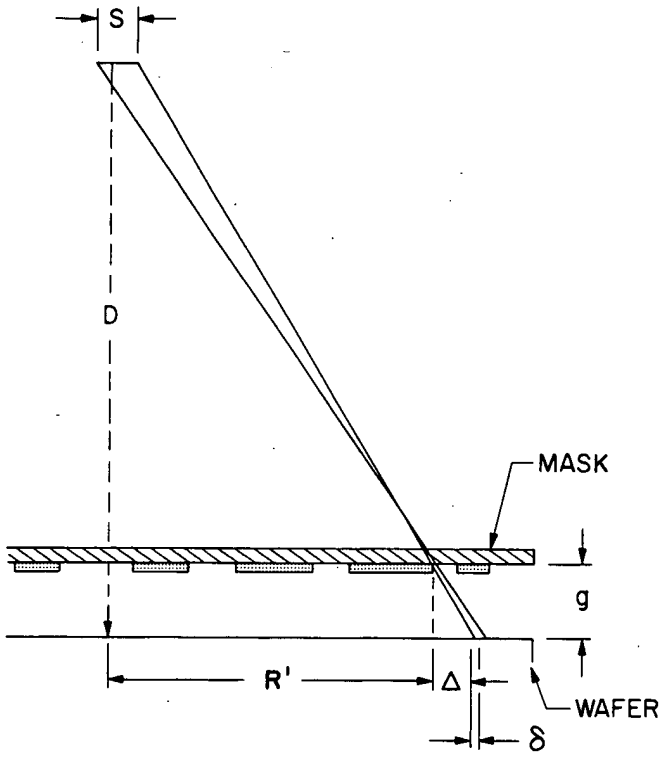

FIGURE 21
X-ray proximity printing.

all points o
tolerance, f
Auton
than 0.1 μn
the mechan
proximity p
Machi
Such others
mask distor

4.4.3 X-r

X-rays are p
The maximu
greater than
atoms of the
In earl
electron-bear
The target m
generation b
input power
limited by th
of diameter
is a typical u
about 10 mW
is proportion
proportional t
the target itsel
a thick target
average, throu
This effect an
an upper limit
Much hi
speed rotating
electron focal
may be tilted c
viewed from t
the larger spot
a relative enh
increase in the
high-power X-
Another
flux, is the pla
by heating a p
radiation consi

all points on the wafer, only that the spatial variations be the same, within close tolerance, for all levels.

Automatic registration is desirable. Automatic systems with precision better than 0.1 μm have been reported. Such precision places stringent requirements on the mechanical design of the alignment stage; the mechanisms found in optical proximity printers are in general not adequate.

Machine imprecision is only one component of the total registration error. Such others as mask stacking errors due to pattern generator placement errors, mask distortion, and wafer process-related contributions also play a role.

4.4.3 X-ray Sources

X-rays are produced by the interaction of incident electrons and a target material. The maximum X-ray energy is the energy E of the incident electrons. If E is greater than the excitation energy E_C of the characteristic line radiation of the atoms of the material, the X-ray spectrum will contain these lines.

In early X-ray lithography experiments, the X-ray source was often an electron-beam evaporator with the chamber modified to accept a mask and wafer. The target metal could be changed easily to modify the X-ray spectrum. X-ray generation by electron bombardment is a very inefficient process; most of the input power is converted into heat in the target. The X-ray flux is generally limited by the heat dissipation in the target. With electrons focused to a spot of diameter 1 mm on an aluminum target on a water-cooled stem, 400–500 W is a typical upper limit for the input power. The X-ray power produced is only about 10 mW, and this power is distributed over a hemisphere. The X-ray power is proportional to the electron current. The power in the line radiation is also proportional to $(E - E_C)^{1.63}$ for a target thin enough that absorption of X-rays by the target itself can be neglected. However, as E increases, the electrons penetrate a thick target more deeply. The characteristic X-rays produced must pass, on the average, through more material on the way out, and are absorbed more strongly. This effect and the extension of the high energy cutoff of the X-ray spectrum set an upper limit for E.

Much higher X-ray fluxes are available from generators which have high-speed rotating targets.[26] The heat dissipation is spread over a larger area; the electron focal spot is on the rim of a spinning, water-cooled wheel. The wheel may be tilted or the rim beveled so that an elliptical focal spot appears round when viewed from the direction of interest. Because more power can be dissipated in the larger spot, source brightness can be increased in this way, at the expense of a relative enhancement of the higher energy portion of the spectrum and some increase in the flux spatial nonuniformity. Reference 26 reviews the status of high-power X-ray generator development.

Another type of source, which is capable of an order of magnitude greater flux, is the plasma discharge source. There are several versions, but all function by heating a plasma to a temperature high enough to produce X radiation. The radiation consists of strong lines superimposed on a weak continuum. The source

is pulsed at a low repetition rate. In one embodiment the source size is 2 mm. Repetition rate is 3 Hz.[33] For FBM-G resist the total time to expose nine 2 cm $\times$ 2 cm fields is 120 seconds. If overhead is 30 seconds, then throughput is 24 wafers / hr. Special problems with such a source are reliability and contamination produced in the plasma chamber.

4.4.4 X-ray Masks

An X-ray mask consists of an absorber on a transmissive membrane substrate. The ratio of metal thickness to substrate thickness is greater than for a photomask. These thicknesses are determined by the transmission of the materials for the X-ray wavelength of interest.

Of the heavy metals with larger ρZ^4 absorbers, gold has been widely used because it is easily patterned. The thicknesses of gold necessary for absorption of 90% of the incident X-ray flux are 0.7 μm, 0.5 μm, 0.2 μm, or 0.08 μm for the X-ray wavelengths 4.4 Å(Pd_L), 8.3 Å(Al_K), 13.3 Å(Cu_L), or 44.8 Å(C_K), respectively. Thus, in general the metal is considerably thicker than the chromium layer on a photomask. Methods for patterning the gold with high resolution include electroplating and ion milling. Electroplating produces excellent definition with vertical walls, but requires a vertical-wall primary pattern in a resist that has a thickness equal to that of the metal to be plated. More often, a subtractive process has been employed in which a thinner resist layer is used to pattern a thin layer of a refractive metal; the refractive metal serves as a mask for ion milling the underlying gold. With this method it has been possible to form walls that depart from the vertical by 20° or less. The minimum linewidth attainable by ion milling in 0.5 μm thick gold is $\sim$ 0.4 μm. For higher resolution, longer wavelengths such as the 13 Å Cu_L radiation may be used where gold thickness can be reduced. Lines as small as 0.16 μm have been replicated with this type of radiation.[34]

The membrane forming the mask substrate should be as transparent to the X-rays as possible, smooth, flat, dimensionally stable, reasonably rugged, and transparent to visible light if an optical registration scheme is used. Materials that have been used include polymers such as polymide and polyethylene terephthalate, silicon, SiC, Si_3N_4, Al_2O_3, and a Si_3N_4–SiO_2–Si_3N_4 sandwich structure. Although different mask substrates are appropriate for different portions of the soft X-ray spectrum, there is not yet general agreement on the best material for any particular wavelength.

The major questions remaining about X-ray masks concern their dimensional stability, minimum attainable defect densities, and ease of handling. Dimensional stability can be degraded by radiation damage produced by the X-ray flux. This also makes the mask substrate optically opaque. Polymer membrane substrates can be distorted locally by the absorber metallization. They are impractical. For greater dimensional integrity a stiffer substrate material is favored. If a plot like that of Fig. 14 is made for a BN X-ray mask, the pattern distortion is typically worse than for the photomask used to produce Fig. 14.

4.4.5 Synchrotron Radiation

Some experiments have been reported in which the synchrotron radiation from electron synchrotrons and storage rings was used for X-ray lithography. The small angular divergence of the radiation simplifies mask-wafer registration, and the high intensity of the radiation leads to short exposure times. A single storage ring could provide radiation to a large number of exposure stations.

In synchrotrons and storage rings, high-energy electrons are forced into closed curved paths by magnetic fields. An electron moving through a perpendicular magnetic field has an acceleration directed toward the center of the orbit and emits radiation. For the high-energy electrons of interest, which have velocities very nearly equal to that of light, the radiation is emitted in a narrow cone in the forward direction of motion of the electron. An observer looking along a tangent to the orbit sees a bright spot. The radiation is very different from that of a point source because of the narrow beam from each electron. The radiation from a circular machine would come from all tangents and have the shape of a disc. The angular divergence of the radiation in the vertical direction is $\psi \approx (1957E)^{-1}$, where E is the electron energy in 1 GeV and ψ is in radians. Thus, for a 1 GeV machine the vertical divergence is only 0.5 mradians.

High-energy electrons are provided to the storage ring by a microtron, a small synchrotron, or a small linear accelerator. The ring is briefly operated as a synchrotron to boost the electron energy to the final value. Then, the electrons may circulate for several hours in a stable orbit. The loss due to the power radiated as synchrotron radiation is compensated by one or more acceleration cavities around the ring. Nevertheless, the current slowly decays because electrons collide with the walls.

The peak of the power spectrum of the synchrotron radiation occurs at wavelength λ_p. This is related to the electron energy E (in GeV) and magnet-bending radius R (in m) by

$$\lambda_p = 2.35\, R/E^3 \tag{24}$$

A 0.83 GeV machine with $R = 2.1$ m would have a power spectrum peaked at $\lambda_p = 8.4$ Å.

During the last few years a Fraunhofer Institute in Berlin has been developing a small storage ring called COSY for X-ray lithography.[35] Figure 22 shows a sketch of this ring. Total floor space required is 30 m^2. Other components of the exposure system are under development elsewhere. For example, the stepper has been constructed by Suss. Alignment accuracy is ± 0.02 μm. COSY will provide a flux density of 250 mW/cm^2. There will of course be several beam lines, each with its own stepper. A similar effort is underway in Japan. The cost of such a facility for volume production of advanced chips would be high, but not prohibitive. The cost of a modern production line is as high as five times the cost of COSY. Special problems include reliability and safety. However, the goal for COSY is 95% up time. The resolution limit of COSY is determined by diffraction. Recall from section 4.2.2 the image of an edge of a feature on a mask used in proximity printing is spread over a distance $\approx 1.3\sqrt{g\lambda/2}$. For COSY this

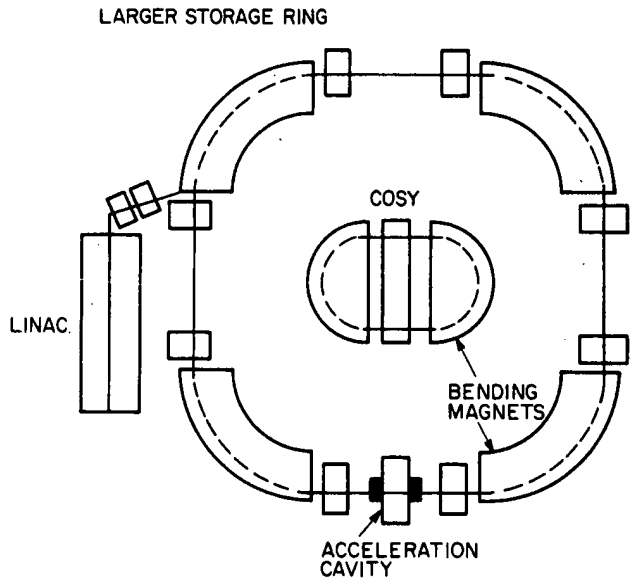

FIGURE 22
Sketch of COSY storage ring for lithography compared in size with a larger conventional ring.

diffraction blur is 0.2 μm. The parameters δ and Δ are much smaller because of the small source size and the small angular divergence of the radiation.

4.4.6 Commercial X-ray systems

Table 6 lists specifications for three commercially available X-ray step-repeat exposure systems.[36,37,38] The first two use conventional electron bombardment X-ray sources. These are automatic systems that can be compared with the optical exposure tools described in a previous section. Resolution of these systems is limited by penumbral blur and by the low-resolution resists that must be used. The third entry in the table has a laser-driven plasma source of very small diameter.[38] The larger X-ray flux of this machine allows the use of better resists. Ultimate

TABLE 6
Three commercial X-ray steppers

	XLS-1000 Perkin Elmer	MX-1600 Micornix	XRL5000 Hampshire
Source	Rotating, W	Pd	plasma
Wavelength (Å)	7.0	4.4	12-14
Gap (μm)	20	25	20
Blur (μm)	0.17	0.35	0.05
Field (mm^2)	$\leq$30 × 30	$\leq$ 50 × 50	14 × 14
Overlay error (μm)	$\pm$0.15(3σ)	$\pm$0.1(2σ)	$\pm$0.1(3σ)
Throughput (wafer/hr)	40, 100 mm*	10, 150 mm†	15–40, 150 mm

*10 mJ/cm^2 resist.
†20 mJ/cm^2 resist (DCOPA).

resolution is limited by diffraction. But practically usable resolution is limited by the accuracy of registration, which is in turn limited by control of the mask-wafer gap (± 0.5 μm).

4.5 ION LITHOGRAPHY

Ion lithography systems are of two types: a scanning focused-beam system and a masked-beam system. When an ion beam is used to expose resist, higher resolution is potentially possible than with an electron beam because of less scattering. In addition, resists are more sensitive to ions than to electrons. There is also the possibility of wafer processing without resists if the ion beam is used to implant or sputter selected areas of the wafer. The most important application is repair of photomasks, a task for which commercial systems are available.

The sensitivity for PMMA resist has been measured for 30 keV, 60 keV, and 200 keV He^+ ions and for 100 keV and 150 keV Ar^+ ions. The dose required for exposure is nearly two orders of magnitude less than with 20 keV electrons.[39] The perpendicular straggle of the path of an ion penetrating material and the range of low-energy secondary electrons produced are less than the range of back-scattered electrons produced in electron lithography. The ion energies for exposing resist depend on the ion. If the ion must penetrate 2500 Å of resist, then a proton would need 14 keV and a Au ion 600 keV for the projected range to be 3000 Å.

For a beam used in fabrication by sputtering, lower energies are generally of interest. When an ion beam is incident on a material, the sputtering yield increases with beam energy for beam energy larger than some small threshold value. There is an energy limit beyond which the yield decreases as the ions penetrate more deeply and fewer surface atoms receive enough energy to leave the surface. For example, the peak in the sputtering curve for Ar^+ ions incident on Cu occurs at 23 keV. For ion implantation, energies from 30 keV to 500 keV are used, and doses range up to 10^{15} ions / cm^2 (or 1.6×10^{-4} C/cm^2 for monovalent ions, representing a much larger dose than for resist exposure).

The problems of ion optics for scanning ion systems are more severe than for electron optics. The brightest sources are the two types of field ionization sources in which ions are produced in the strong field near a pointed tungsten tip. The source of ionized material is a gas surrounding the tip or a liquid metal that flows to the tip from a reservoir. The largest current densities obtained in the focused image of such a source are 1.5 A / cm^2 for Ga^+ in a 0.1 μm spot and 15 mA/cm^2 for H^+ in a 0.65 μm spot.[40,41] Total beam current is severely limited. There are no bright sources for such useful implant species as B and P. Electrostatic lenses rather than magnetic must be used for focusing ion beams. If a magnetic lens were used to focus an ion beam, the field would have to be much larger than in the electron optics case since from Eq. 13 the required field is proportional to $(mV/f)^{\frac{1}{2}}$, where m is the particle mass. Different isotopes would be focused to different points. Similarly, magnetic deflection is much less practical than electrostatic. Electrostatic optical systems generally have higher aberrations, necessitating small aperture α and small scan fields.

A prototype scanning system has been reported in which a beam of 57 keV Ga^+ ions is focused to a 0.1 μm diameter spot with current density 1.5 A/cm^2.[40] Spot size is apparently limited by chromatic aberration of the electrostatic lens and the large 14 eV energy spread of the source. There is also work on use of collimated ion beams with stencil masks. Some workers have employed a collimated 500 eV Hg^+ beam to transfer a pattern by sputter etching.[42]

Mask-based systems are of two types. One type is a 10X-reduction projection step-repeat system which projects 60–100 keV light ions through a stencil mask.[43] Overlay accuracy is $\pm 0.05\mu$m. The major disadvantage is the fragile foil mask which can treat re-entrant patterns only by double exposure with two masks.

The second type is a step-repeat proximity printer in which 300 keV protons are projected through the 0.5 μm thick portions of an all-silicon mask.[44] The mask is aligned so that the ions travel along the channels in the <100> direction. Projected throughput is sixty 100-mm wafers/hr, and the overlay error is $\sim 0.1\mu$m—barely adequate for 0.5 μm lithography. Resolution is set by scattering of the ions as they emerge from the channels. Edge resolution is 0.1 μm for the beam-scattering angle of 0.3°. The main disadvantage is the fragile mask with the 0.5 μm membrane. However, if a large fraction of the mask consists of the thicker silicon absorber, then the mask may be sufficiently rugged. The highest resolution in resists is obtained with a stencil mask and a beam of protons of energy 40 to 80 keV. Lines as fine as 400 Å have been printed in this way.[45]

4.6 SUMMARY AND FUTURE TRENDS

Optical lithography will continue to improve with wavelengths approaching 190 nm, the limit for silica. Even if reflective optics are employed, the radiation must still penetrate the mask. The optical wafer stepper will be the lithography system of choice for many years because of its relative simplicity, convenience, and reasonably high throughput. The practical resolution limit in production applications will be 0.5 μm or slightly lower. This resolution will be needed for MOS production by 1992. It will be available. As we have seen, the main barriers to higher optical resolution are (1) optical materials, (2) small depth of focus, and (3) the difficulty of obtaining diffraction-limited imaging over a large field.

Custom circuits and experimental devices for which high throughput is not needed will continue to be patterned by scanning electron-beam systems. In these applications fine definition, good overlay, flexibility, and quick turnaround are of primary importance. The main disadvantages of scanning systems are complexity and low throughput. Although impressive increases in throughput and reliability have been made by Japanese manufacturers of these systems, there is still the formidable problem that throughput is roughly inversely proportional to the square of the linewidth.

Finally, there is the application of a new lithographic method to high-volume production of advanced circuits with dimensions beyond the optical limit. There

FIGURE
Resolutio
considerec

are seve
masked
advantag
It is not
possible
familiar
are indic
regime o
ion proxi
lower thr
At
schemes
a rapid, c
Single-la
As highe
would the
patterning
and subtr
etching.
cessing (
out a nev
The new

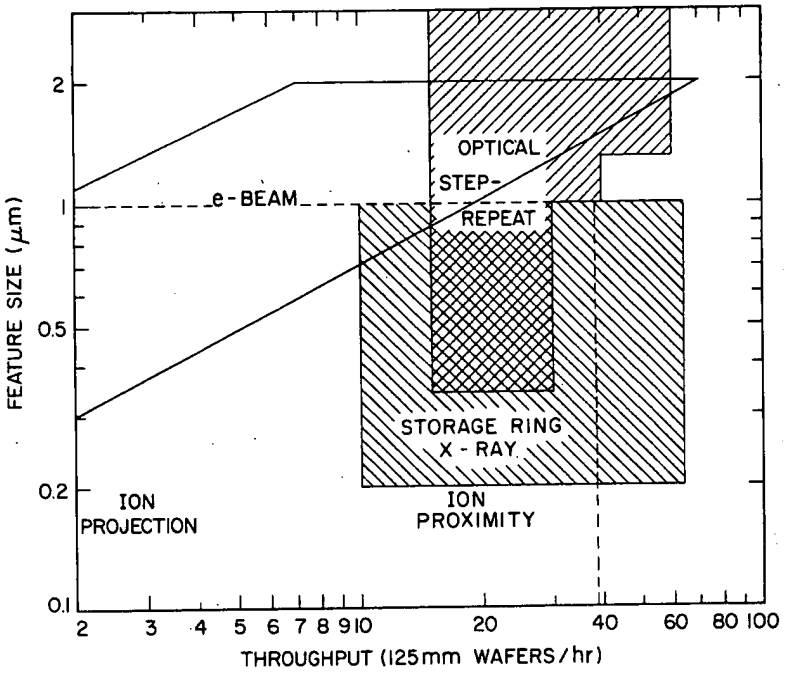

FIGURE 23
Resolution and throughput in the submicron regime. The boundaries of each region should be considered fuzzy.

are several candidates for this task: X-ray lithography with storage ring source, masked ion-beam lithography, and possibly electron proximity printing. The advantages and disadvantages of each have been discussed in previous sections. It is not yet possible to predict which will meet with success, just as it is not yet possible to predict with certainty the limit of miniaturization for the much more familiar MOS circuit technology. Some projections of resolution and throughput are indicated in Fig. 23. The rectangle bordered by the dashed lines indicates the regime of ion lithography. No boundary is shown between the ion projection and ion proximity printing regions. In general, the present projection machines have lower throughput than the proximity printers.

At present, resists are needed for all forms of lithography. Multilayer resist schemes are capable of high resolution. They will not find wide acceptance unless a rapid, convenient, production-worthy method of processing them is developed. Single-layer resist is also capable of high resolution with useful thickness.[46] As higher resolution is sought, resists may disappear. Indeed, lithography itself would then disappear and be combined with processing. New schemes combining patterning and formerly separate processing techniques would be both additive and subtractive in contrast with the present, nearly exclusive, use of subtractive etching. This development will be slow because the disdavantage of resist processing (application, developing) will be replaced by the necessity of working out a new technique for each material (polysilicon, SiO_2, $Ga_xAl_{1-x}As$, etc.). The new methods required for the sub-0.1 μm region will of course depend on

the nature of the new circuit technologies that will replace MOS, bipolar, and GaAs MESFET designs.

PROBLEMS

1 Derive Eq. 6, $H(u) = \frac{2}{\pi}[\cos^{-1}(u/u_m) - (u/u_m)\sqrt{1-(u/u_m)^2}]$, using the figure and simple geometrical considerations.

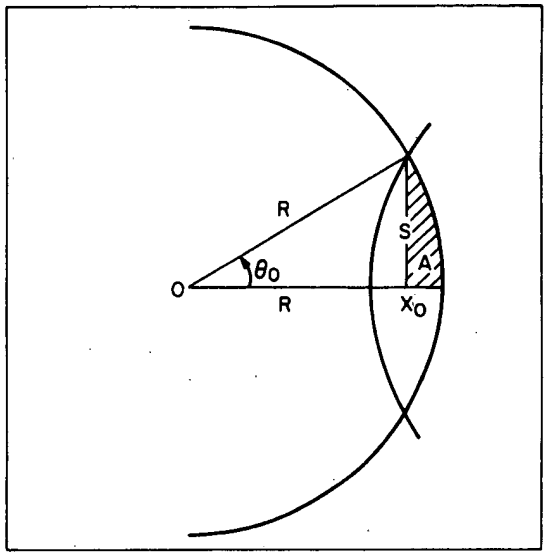

2 Suppose that you are required to specify the resist thickness that will be used in a production lithographic process. The following data are available:

- 1.5 μm minimum features must be printed. Resolution is adequate when the resist thickness T is in the range 0.5 to 2.0 μm, but feature size control is better for thinner resists.
- Each wafer has 150 chip sites; each chip has a 0.2 cm^2 active area.
- Five mask levels are required to complete the device.
- 2000 finished wafers must be produced each day (20 hr per day = 3 shifts).
- The resist defect density D_0 increases as the resist is made thinner, where D_0 is the number of defects per square centimeter, and is approximated by $D_0 = 1.4\ T^{-3}$. T is in microns.
- The chip yield (percentage good) can be approximated at each mask level by $y = (1 + qD_0a)^{-1}$, where q is the fraction of defects that render a chip inoperable (fatality rate) and a is the active area of the chip.
- On average, 50% of the defects are fatal defects.
- More time is needed to expose thick resist than to expose thin resist. The exposure tool throughput in wafers/hr is approximated by $125 - 50T$ for ($0.5 \leq T \leq 2.0$ μm).

(a) Specify the resist thickness to be used and justify your recommendation with tabular and graphical data.

(b) If exposure tools cost $350,000 each, what is the difference in equipment cost for a process using 1 μm and 1.5 μm of resist?

3 In electron beam lithography the term *Gaussian beam diameter* (d_G) describes the diameter of an electron beam in the absence of system aberrations, that is, a beam distorted only by the thermal velocities of the electrons. The current density in a Gaussian beam is given by $J = J_p \exp[-(r/\sigma)^2]$, where J_p is the peak current density, r is the radius from the center of the beam, and σ is the standard deviation of electron distribution in the beam. Defining $d_G = 2\sigma$, derive an expression relating d_G to the peak current density J_p and the total current in the electron beam I.

Answer: $I = (\pi/4)J_p d_G^2$

4 The maximum current density J_m that can be focused towards a spot with a convergence half-angle α is limited by the transverse thermal emission velocities of the electrons in a Gaussian electron beam. J_m is given by the *Langmuir limit equation*

$$J_m = J_c\left(1 + \frac{eV_0}{kT_c}\right)\sin^2\alpha$$

where J_c is the cathode (source) current density, T_c is the temperature corresponding to the electron energy, k is Boltzmann's constant (1.38×10^{-23}J/K), and e is the electronic charge (1.6×10^{-19}C). For small convergence angles α, derive an expression that relates the Gaussian beam diameter d_G to the electron source parameters J_c, T_c, and V_0.

Answer: $d_G^2 \geq IkT_c/[(\pi/4)J_c e V_0 \alpha^2]$

5 **(a)** The brightness β of a source of electrons is defined as the current density J emitted per unit solid angle Ω, that is, $\beta = J/\Omega$. The units of β are amperes per square centimeter per steradian. Assume that the current is emitted from (or coverages toward) a small area through a cone of included half-angle α and that α is small. Derive an expression relating the maximum source brightness to the source parameters J_c, T_c, and V_0.

Answer: $\beta \approx J_c e V_0/\pi k T_c$

(b) Assuming that brightness is conserved in the electron beam column, show that the Gaussian beam diameter d_G is related to the source brightness.

Answer: $d_G \approx (2/\pi)(1/\alpha)(I/\beta)^{1/2}$

6 Suppose that an x-ray resist must see a mask modulation greater than or equal to 0.6 in order to form useful resist images. What is the minimum gold thickness required on an x-ray mask to satisfy this requirement if the exposure wavelength is 4 Å?

Answer: $T \leq 0.31\ \mu$m

REFERENCES

1 F. H. Dill, W. P. Hornberger, P. S. Hauge, and J. M. Shaw, "Characterization of Positive Photoresist," *IEEE Trans. Electron Devices*, **ED-22**, 445 (1975).

2 R. K. Watts and N. G. Einspruch, Eds., *Lithography for VLSI, VLSI Electronics: Microstructure Science*, Vol. 16, Academic Press, New York, 1987.

3 H. I. Smith, N. Enfremow, and P. L. Kelley, "Photolithographic Contact Printing of 4000 Å Linewidth Patterns," *J. Electrochem. Soc.*, **121**, 1503 (1974).

4 W. N. Jones, "A Far Proximity Photolithographic Process for Semiconductor Manufacture," *Proc. Microelectronics Sem. Kodak Interface*, **75**, 49 (1976).
5 B. J. Lin, "Deep UV Lithography," *J. Vac. Sci. Technol.*, **12**, 1317 (1975).
6 J. G. Skinner, "Some Relative Merits of Contact, Near-Contact, and Projection Printing," *Proc. Microelectronics Sem. Kodak Interface*, **73**, 53 (1974).
7 Y. Nakane, T. Tsumori, T. Mifune, "Deep UV Photolithography," *Proc. Microelectronics Sem. Kodak Interface*, **78**, 32 (1978).
8 D. A. McGillis and D. L. Fehrs, "Photolithographic Linewidth Control," *IEEE Trans. Electron Devices*, **ED-22**, 471 (1975).
9 R. C. Heim, "Practical Aspects of Contact / Proximity Photomask / Wafer Exposure," *Proc. SPIE*, **100**, 104 (1977).
10 M. Born and E. Wolf, *Principles of Optics*, 5th Ed., Pergamon Press, New York, 1975.
11 M. C. King and M. R. Goldrick, "Optical MTF Evaluation Techniques for Microelectronic Printers," *Solid State Technol.*, **20**, 37 (1977).
12 M. A. Narasimham and J. H. Carter, Jr., "Effects of Defocus on Photolithographic Images Obtained with Projection Printing Systems," *Proc. SPIE*, **135**, 2 (1978).
13 H. Moritz, "High Resolution Lithography with Projection Printing," *IEEE Trans. Electron Devices*, **ED-26**, 705, (1979).
14 J. H. Bruning, "Performance Limits in 1:1 UV Projection Lithography," *J. Vac. Sci. Technol.*, **16**, 1925 (1979).
15 V. Pol, J. H. Bennewitz, G. C. Escher, M. Feldman, V. A. Firtion, T. E. Jewell, B. E. Wilcomb, and J. T. Clemens, "Excimer Laser-Based Lithography: A Deep Ultraviolet Wafer Stepper," *Proc. SPIE*, **633**, 6 (1986).
16 R. D. Moore, "E-Beam Direct Writing in Manufacturing," *Proc. Symp. Electron and Ion Beam Technol.*, St. Louis, May 1980, p. 126.
17 L. F. Thompson, C. G. Wilson, and M. J. Bowden, Eds., *Introduction to Microlithography*, ACS, Washington, D.C., 1983.
18 J. M. Moran and D. Maydan, "High Resolution, Steep Profile Resist Patterns," *J. Vac. Sci. Technol.*, **16**, 1620 (1979).
19 T. H. P. Chang, A. D. Wilson, C. H. Ting, R. Viswanathan, M. Parikh, and E. Munro, "The Probe Forming and Deflection System for Vector Scan 1 E-B Lithographic System," *Proc. Symp. Electron Ion Beam Sci. Technol.*, Princeton, May 1976, p. 377.
20 D. R. Herriott, R. J. Collier, D. S. Alles, and J. W. Stafford, "EBES: A Practical Electron Lithographic System," *IEEE Trans. Electron Devices*, **ED-22**, 385 (1975).
21 D. S. Alles, C. J. Biddick, J. H. Bruning, J. T. Clemens, R. J. Collier, E. A. Gere, L. R. Harriott, F. Leone, R. Liu, T. J. Mulrooney, R. J. Nielsen, N. Paras, R. M. Richman, C. M. Rose, D. P. Rosenfeld, D. E. A. Smith, and M. G. R. Thomson, "EBES4-A New Electron Beam Exposure System," *J. Vac. Sci. Technol.*, **B5**, 47 (1987).
22 H. C. Pfeiffer, "Recent Advances in Electron-Beam Lithography for the High-Volume Production of VLSI Devices," *IEEE Trans. Electron Devices*, **ED-26**, 663 (1979).
23 R. Ward, A. R. Franklin, I. H. Lewin, P. A. Gould, and M. J. Plummer, "A 1:1 Electron Stepper," *J. Vac. Sci. Technol.*, **B4**, 89 (1986).
24 P. Nehmiz, W. Zapka, U. Behringer, M. Kallmeyer, and H. Bohlen, "Electron Beam Proximity Printing: Complementary Mask and Level-to-Level Overlay with High Accuracy," *Proc. Symp. Electron, Ion, Photon Beams*, Tarrytown, NY, May 1980, p. 136.
25 D. L. Spears and H. I. Smith, "High Resolution Pattern Replication Using Soft X-rays," *Electronics Lett.*, **8**, 102 (1972).
26 M. Yoshimatsu and S. Kozaki, "High Brilliance X-ray Sources," in *X-ray Optics*, H. J. Queisser, Ed., Springer, Berlin, 1977.
27 S. Yamazaki, S. Nakayama, T. Hayasaka, and S. Ishihara, "X-ray Exposure System Using Finely Position Adjusting Apparatus," *J. Vac. Sci. Technol.*, **15**, 987 (1978).
28 T. Hayashi, "Electron Beam and X-ray Lithography for VLSI Devices," *Proc. Symp. Electron Ion Beam Technol.*, Seattle, May 1978, p. 85.
29 R. K. Watts, K. E. Bean, and T. L. Brewer, "X-ray Lithography with Aluminum Radiation and SiC Mask," *Proc. Symp. Electron Ion Beam Technol.*, Seattle, May 1978, p. 453.

30 J. H. McCoy, "X-ray Lithography for Integrated Circuits—A Review," *Proc. SPIE*, **100**, 162 (1977).
31 J. R. Maldonado, M. E. Poulsen, T. E. Saunders, F. Vratny, and A. Zacharias, "X-ray Lithography Source Using A Stationary Solid Pd Target," *J. Vac. Sci. Technol.*, **16**, 1942 (1979).
32 G. A. Wardley, R. Feder, D. Hofer, E. E. Castelanni, R. Scott, and J. Topalian, "X-ray Lithography," *Circuits Mfg.*, **15**, 30 (1978).
33 I. Okada, Y. Saitoh, S. Itabashi, and H. Yoshihara, "A Plasma X-ray Source for X-ray Lithography," *J. Vac. Sci. Technol.*, **4**, 243 (1986).
34 D. C. Flanders and H. I. Smith, "Surface Relief Gratings of 3200 A Period, Fabrication Techniques and Influence on Thin Film Growth," *J. Vac. Sci. Technol.*, **15**, 1001 (1978).
35 A. Heuberger, "X-ray Lithography," in *Microcircuit Engineering 85*, K. B. van der Mast and S. Radelaar, Eds., Elsevier, Amsterdam, 1985.
36 B. S. Fay and W. T. Novak, "Advanced X-ray Alignment System," *Proc. SPIE*, **632**, 146 (1986).
37 R. B. McIntosh, Jr., G. P. Hughes, J. L. Kreuzer, and G. R. Conti, "X-ray Step-and-Repeat Lithography System for Submicron VLSI," *Proc. SPIE*, **632**, 156 (1986).
38 R. D. Frankel, J. P. Drumheller, A. S. Kaplan, and M. J. Lubin, "X-Ray Lithography Process Optimization Using a Laser-Based X-Ray Source," *Proc. Microelectronics Sem. Kodak Interface*, **86**, 82 (1987).
39 M. Komuro, N. Atoda, and H. Kawakatsu, "Ion Beam Exposure of Resist Materials," *J. Electrochem. Soc.*, **126**, 483 (1979).
40 R. L. Seliger, J. W. Ward, V. Wang, and R. L. Kubena, "A High Intensity Scanning Ion Probe with Submicrometer Spot Size," *Appl. Phys. Lett.*, **34**, 310 (1979).
41 J. Orloff and L. W. Swanson, "A Scanning Ion Microscope with a Field Ionization Source," in *Scanning Electron Microscopy*, ITT Res. Inst., Chicago, 1977, p. 57.
42 B. A. Free and G. A. Meadows, "Projection Ion Lithography with Aperture Lenses," *J. Vac. Sci. Technol.*, **15**, 1028 (1978).
43 G. Stengl, H. Löschner, W. Maurer, and P. Wolf, "Ion Projection Lithography Machine IPLM-01: A New Tool for Sub 0.5 μm Modification of Materials," *J. Vac. Sci. Technol.*, **B4**, 194 (1986).
44 J. L. Bartelt, "Masked Ion Beam Lithography: An Emerging Technology," *Solid State Technol.*, **28**, 215 (1986).
45 J. N. Randall, D. C. Flanders, N. P. Economou, J. P. Donnelly, and E. I. Bromley, "Masked Ion Beam Resist Exposure Using Grid Support Stencil Masks," *J. Vac. Sci. Technol.* **B3**, 58 (1985).
46 M. Sasago, M. Endo, Y. Hirai, K. Ogawa, and T. Ishihara, "Half-Micron Photolithography Using A KrF Excimer Laser Stepper," *Proc. IEDM*, 316 (1986).
47 R. K. Watts, "Advanced Lithography" *Very Large Scale Integration, Fundamentals and Application*, Ed. D F. Barbe, Springer, New York, 1982, Chapter 2.